magnetochemistry

MDPI

Review

Recent Advances in Magnetic Nanoparticles and Nanocomposites for the Remediation of Water Resources

Joseph Govan

Department of Engineering and Soils, Faculty of Agricultural Sciences, University of Chile, Santiago 8320000, Chile; joseph.govan@uchile.cl

Received: 13 August 2020; Accepted: 22 September 2020; Published: 9 October 2020

Abstract: Water resources are of extreme importance for both human society and the environment. However, human activity has increasingly resulted in the contamination of these resources with a wide range of materials that can prevent their use. Nanomaterials provide a possible means to reduce this contamination, but their removal from water after use may be difficult. The addition of a magnetic character to nanomaterials makes their retrieval after use much easier. The following review comprises a short survey of the most recent reports in this field. It comprises five sections, an introduction into the theme, reports on single magnetic nanoparticles, magnetic nanocomposites containing two of more nanomaterials, magnetic nanocomposites containing material of a biologic origin and finally, observations about the reported research with a view to future developments. This review should provide a snapshot of developments in what is a vibrant and fast-moving area of research.

Keywords: nanomaterials; nanocomposites; nanotechnology; magnetic nanomaterials; water treatment; environmental remediation; catalysis; adsorption; biological materials

1. Introduction

Water is an important part of the global resources necessary for agriculture, industry and the maintenance of human health [1]. However, many of the sources from which it is extracted for different uses have been found to be contaminated with substances which either make it harmful for human life (Table 1) or in other ways unsuitable for use. Some of this contamination can be from natural sources or as a product of human activity [2], be it from agriculture, industry or domestic activity [3]. For all these reasons there is a strong demand for the development of new methods for the removal of contaminants from water sources with two goals, for its potential reuse and for preventing damage to the environment when this water is discharged [4].

Table 1. Examples of classes of contaminants found in water sources. Sourced from Moothi et al. [5] and adapted.

Category of Contaminant	Subcategory	Selected Examples	Permitted Level ($mg \cdot L^{-1}$)	Examples of Sources	Examples of Known Health Effects
Inorganic	Heavy metals	cadmium (Cd) lead (Pb) copper (Cu)	0.005 0.015 0.05	Mining and petroleum industries	Cancer, Cardiovascular disease, diabetes
	Polyatomic	Arsenate (AsO_4^{3-}) Chromate (CrO_4^{2-}) Nitrate NO_3^-	0.05 0.05 50	Agricultural and steel industries	Renal failure, hypertension, Skeletal malformation

Table 1. *Cont.*

Category of Contaminant	Subcategory	Selected Examples	Permitted Level (mg·L^{-1})	Examples of Sources	Examples of Known Health Effects
Organic	Dyes	methylene blue crystal violet	0.01 * 20.8 **	Textile and Printing Industries	Mutagenicity, Genotoxicity, Cancer
	Herbicides	2,3-dichlorophenol	0.01 ***	Agriculture	
	Pharmaceuticals	ibuprofen	NA	Pharmaceutical industry	
Microorganisms	Bacteria	Escherichia coli	1000 $^{+}$	Fecal and soil pollution	Waterborne diseases, diarrhea
	Viruses	Poliovirus-1	0 $^{++}$		

Maximum values sourced from the EPA Ireland [6] except where otherwise stated. Guide for additional symbols: * Methylene Blue maximum concentration in mg.kg^{-1} for aquatic products [7]. ** Maximum predicted no Effect Concentration for Crystal Violet [8]. *** Florida state drinking guidelines for 2,3-dichlorophenol [9]. $^{+}$ number of organisms per 100 mL, $^{++}$ number of plaque forming units per 10 L.

Nanomaterials are a highly interesting class of materials with many potential applications ranging from sensors [10], display technologies [11], polymer reinforcement [12], catalysis [13], to nanomedicine [14]. Nanomaterials have been reported as materials for the removal of contaminating chemicals from water [5,15,16]. Due to their small size, nanoparticles are readily dispersed in liquid where, due to their large surface area, they have a formidable potential to interact with contaminants in liquid media. Consequently, nanomaterials show exceptional promise for the reduction of contaminants in water. Two of the main forms of processes by which this can occur are:

1. The adsorption of the contaminant on the surface or internal structure of the adsorbent [17,18]. This process does not chemically alter the nature of the contaminant and provides the potential for the subsequent desorption and concentration of the contaminant, a process which can be used to isolate in an economical way select contaminants [19].
2. Catalytic degradation. This is a term for a whole series of different chemical processes initiated or mediated by the presence of the catalyst. There are many different classes of catalytic activity which have been reported for nanomaterials in relation to removal of contaminants from water such as photocatalysis [20], reduction [21] and catalysis of the activation of oxidant species [22].

While nanomaterials can be an important tool for the removal of contaminants from water, nanomaterials themselves can be act as contaminants. This is due to nanoparticles being potentially damaging to the environment and human health both as particles themselves and as an effect of potentially toxic products coming from their degradation in the environment [23]. In addition, nanomaterials may still be active and would be effective for reuse or may be made so through some form of processing [24]. As a result of these facts, complete removal of nanoparticles from water resources after their use in the removal of contaminants is an important research goal. Traditional methods involve the incorporation of nanomaterial into membranes [25] or aggregation of the nanoparticles followed by sedimentation as well as more advanced methods such as filtration through extremely fine media [26]. However, there are issues with either method. Incorporation into membranes reduces the effective surface area of the nanomaterials eliminating one of the primary benefits of this class of material and the use of membranes, filters or similar methods all require specific infrastructure which would increase the cost of processing and make these methods unsuitable for large-scale processing of water.

One potentially interesting property of nanomaterials which could be used in the retention of nanoparticles would be the expression of superparamagnetism in particles of magnetic materials below a certain size [27]. This property means that magnetic nanoparticles have no residual hysteresis in the absence of a magnetic field. Because of this, there is no residual magnetism induced aggregation, which will aid in the dispersion of these nanomaterials in liquid medium. However, when a magnetic field is present the nanoparticles all magnetize and aggregate [27]. This provides essentially an on

and off switch for dispersibility, a property which has been promoted for application in catalysis [28], biologic sensing and drug delivery [29].

For similar reasons, magnetic nanomaterials also demonstrate potential for the remediation of water resources due to their magnetic properties, which would enable dispersion in potentially large bodies of water followed by the application of a magnetic field for retrieval and potential reuse. This is an area that shows great activity, with multiple reviews on the subject being published right up to the present day [30–35]. Nevertheless, with the field advancing at the rate that it is with novel research being published on a daily basis, up-to-date reviews would be an important contribution.

When examining magnetic nanoparticles and nanocomposites for potential application in water remediation the following characteristics would be considered important:

1. Strong magnetic response. This will enable the rapid recovery of the nanomaterial from suspension and prevent loss of the nanomaterial to the environment.
2. High rate of removal of contaminant. This may be due to effective adsorption of the contaminant or strong catalytic activity against the contaminant species.
3. Rapid reuse. After recovery it would be important that the nanomaterial could be readily reused with the minimum of processing. In the case of catalytic nanomaterials, they may be re-utilizable immediately while adsorbent nanomaterials may require adsorbed contaminants be removed or desorbed through elution or other processes.
4. Stability. It would be required that the nanomaterials do not degrade and maintain good performance through multiple cycles of use. This is necessary to ensure that both the target contaminant is removed and the degradation products from the nanomaterial do not contaminate the water resource.

A nanomaterial which demonstrates good examples of these characteristics would show excellent potential as agents for the remediation water. It is likely however that further development would be needed in any case.

The present study aims to provide a review of recently published works in the generation of novel magnetic nanomaterials for use in the remediation of water resources. The review is divided into three main sections separated by the class of nanomaterial that was investigated in the reported research. These classes of nanomaterial will include

1. Single nanoparticle materials: These consist of a single type of nanomaterial. In this section, nanomaterials which have been modified through ligand exchange or through chemical modification of their ligand sphere are included;
2. Magnetic nanocomposite materials: these consist of more than one class of nanomaterial in which one of these materials would be magnetic. This class of material can combine the properties of its various components acting synergistically to perform their function;
3. Magnetic biologic composites: these are specific composite materials where a magnetic nanoparticle is mixed with either cells or with other material of biologic origin. These composites can mix the magnetic activity of these nanomaterials with the processes initiated by the biologic material in order to perform their function.

The review is finalized with observations on the possible future direction in the field of magnetic nanomaterials for water remediation.

Ongoing research into this class of nanomaterial is important for the future development of novel nanomaterials for the remediation of water resources.

2. Single Magnetic Nanoparticle Materials

Single magnetic nanoparticle materials are among the simplest nanomaterials to be included in this review as there is no need for the addition of more than one form of nanomaterial which may complicate the overall synthesis. Numerous shapes and compositions of singular magnetic nanoparticles have been reported recently (Table 2).

Table 2. Examples of distinctive single magnetic nanoparticles detailing their composition, structure, surface area, method for synthesis, contaminant examined and proposed method of removal of contaminant.

Material	Morphology	Surface Area m^2 g^{-1}	Synthesis Method	Contaminant	Method of Removal	Ref
Fe_3O_4	Ultrafine wires	94.43	Co-precipitation	Cd^{2+}, Cu^{2+} Ni^{2+}	Adsorption	[36]
Fe_3O_4	Nanorings	109.3	Hydrothermal synthesis	Methylene blue, rhodamine B and bromophenol blue	Fenton style catalysis	[37]
Mn/Fe oxycarbide	Rod-Like	179.6	Solvothermal synthesis + calcination	Butyl parabens	PMS activation	[38]
Fe_3O_4@C–COOH	Hollow spheres	N/A	Solvothermal synthesis	Pb^{2+} derived from contaminated soils	Adsorption	[39]
$Ni_xMg_yZn_{(1-x-y)}Fe_2O_4$	Spherical	91.6	Ethanol mediated combustion + calcination	Methylene blue dye	Adsorption	[40]
$Mn_xZn_{(1-x)}Fe_2O_4$	Particles	N/A	Co-precipitation	Reactive yellow 15 dye	Photocatalytic Fenton reaction	[41]
Cu–nFe_3O_4	Octagonal	83.7	Co-precipitation	Chlorotetracycline	Catalytic degradation	[42]
$ZnFe_{0.8}Co_{0.4}O_{2.4}$	Hexagonal	10.6	Sol–gel combustion	Bisphenol A and diphenhydramine	PMS activation	[43]
$FeMnO_3$	Porous plate	11.2	Sol–gel combustion	*Bacillus subtilis* bacteria	Mn mediated cell disruption	[44]
$Mn_{0.5}Zn_{0.5-x}Mg_xFe_2O_4$	Spherical	8.3	Sol–gel + sintering	Rhodamine B various bacterial species	Photocatalytic oxidation	[45]
$Ni_{0.6}Zn_{0.4}Fe_2O_4$ and $Ni_{0.6}Zn_{0.2}Ce_{0.2}Fe_2O_4$	Cubic	20.3 23.6	Sol gel+ calcination	various bacterial species	Ion release mediated cell disruption	[46]
Zero valent iron (nZVI)	Spherical	33	Borohydride reduction	Congo red dye	Catalytic reduction	[47]
Sulfur-modified nZVIs (S–nZVIs)	Particles	N/A	Ball-milling	Acetaminophen and ren sulfadiazine	PMS activation	[48]
Carbon-modified nZVIs	Flakes	6.6	Ball-milling	Trichloroethylene	PMS activation	[49]
Fe_3O_4	Nano needles	23.4	Chemical reduction	Pb^{2+}	Adsorption	[50]

2.1. Control of Magnetic Nanoparticle Formation and Behavior in Suspension

The following are examples of reports of methods to control the morphology of magnetic nanoparticles in the synthesis phase. It also includes an investigation into the use of the external environment such as magnetic fields for the recovery of magnetic nanoparticles.

The control of the surface properties is highly important for the utilization of superparamagnetic iron oxide nanoparticles (SPIONs) (average size, 15 nm) in water remediation among other applications. In a report by Oluwatobi et al. [51] various forms of SPION were made using glucose as a stabilizing agent. Through variations in the synthesis control of nanoparticle crystallinity, porosity, and magnetic properties can be achieved. This would be important in the development of particles with the best properties for the remediation of water.

Ultrafine magnetite nanoparticles (size range 4–17 nm) were generated through a co-precipitation reaction by Long et al. [36] who then demonstrated the use of these nanoparticles for the removal of metal ions from river water. As part of the synthesis, surfactants were deliberately omitted. As a result, individual nanoparticles were noted to aggregate into a porous structure. These structures were capable to removing lead (Pb^{2+}), cadmium (Cd^{2+}), copper (Cu^{2+}) and nickel (Ni^{2+}) ions from river water both when added singly or when added simultaneously though there is a drop in performance in the latter case. Maximum adsorbance efficiencies of 85, 79, 83 and 66 $mg{\cdot}g^{-1}$, were reported for Pb^{2+}, Cd^{2+}, Cu^{2+} and Ni^{2+}, respectively. The reuse of the nanoparticles over five cycles was reported after elution of metal ions with dilute nitric acid.

The maximization of the recovery of magnetic nanoparticles through the use of an assembly of permanent magnets was reported by Wong et al. [52] who designed a device for the purpose of the recovery of magnetite (Fe_3O_4). The use of high gradient magnetic separation allows a large rate of recovery of nanoparticles after adsorbance of arsenic with >94% of the particles being captured in the device and >80% of this material being then extracted from the device with desorption permitting further reuse. It is envisaged that such a system may be suitable for use in large-scale water treatment facilities for the removal of arsenic from natural water sources.

Another controlled synthesis of magnetite nanoparticles was reported by Angelico et al. [53] who used an O_2 free synthesis to create nanoparticles with differences in morphologies ranging from spheres to octahedrons (sizes ranging from ~30–120 nm). They tested these different nanoparticles for their adsorption capabilities of As(V) species from water and observed that the presence of increased surface roughness provided increased space for surface binding.

A ring-shaped Fe_3O_4 magnetic nanoparticle was generated by Yang et al. [37] through a hydrothermal synthesis. These nanorings (full diameter, ~155 nm, ring thickness, ~40 nm) were demonstrated as a catalyst for the degradation of organic dyes such as methylene blue, Rhodamine B and bromophenol blue showing excellent activity against all dyes and were showed to retain 85% activity through ten cycles of recovery and reuse. Through EPR and scavenger reactions it was determined that the degradation was through a Fenton style reaction.

Rod-shaped manganese iron oxycarbide were synthesized by Fu et al. [38] through a mixture of solvothermal process and calcination. These rods had an average width of 600 nm and a length of up to 20 μm and were composed of a porous network and irregular crystals (average size 8–17 nm). These particles were investigated for the production of reactive oxygen species (ROS) through activation of peroxymonosulfate (PMS) (Figure 1) that was then used for the degradation of the antimicrobial preservative butyl parabens. A 125 $mg{\cdot}L^{-1}$ solution of the toxin was degraded over 2 h at pH greater than 5. When the butyl parabens were diluted in environmental water samples with the additional dissolved solutes the rate of degradation was increased with up to 83% loss over 45 min compared to 71% reported at the same time for deionized water.

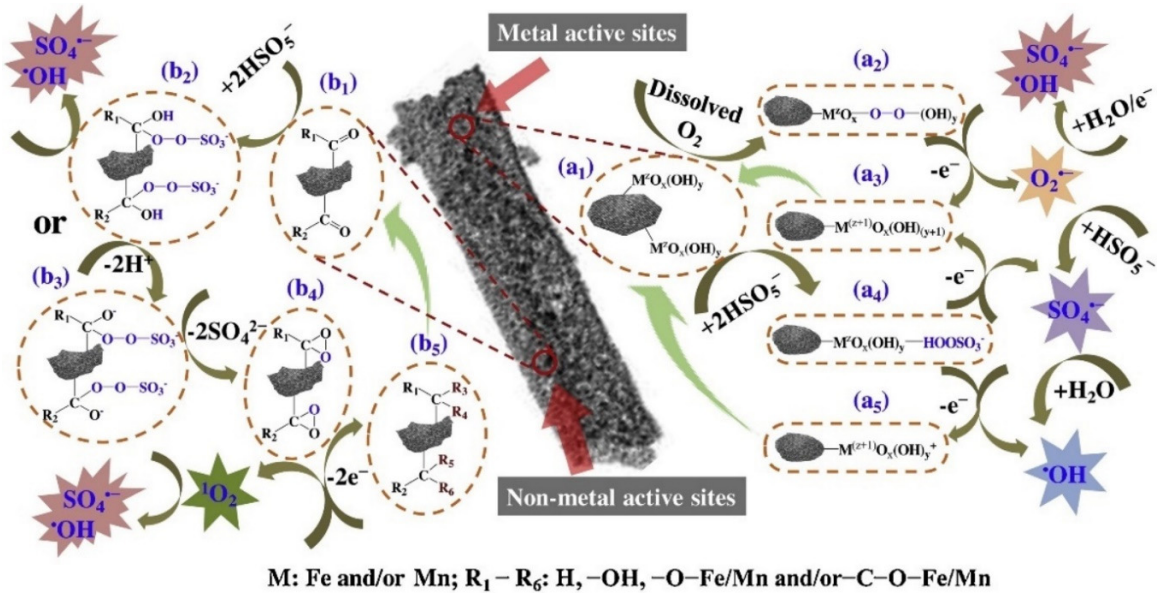

Figure 1. Proposed mechanism for peroxymonosulfate (PMS) activation by rod-shaped manganese iron oxycarbide and ROS formation. Reprinted from Fu et al. [38] with permission from Elsevier.

2.2. Surface Modification of Magnetic Nanoparticles

In the following, magnetic nanoparticles have been modified postsynthetically through reactions with other chemical species to change the surface properties of the nanomaterial. This has been demonstrated to have potential for aiding the removal of contaminants from water.

Surface modification of nanoparticles in order to better target contaminants or other solute species has been reported by Mohammadi et al. [54] who modified Fe_3O_4 nanoparticles (size range 25–42 nm) with epoxy-triazinetrione. This surface functionalization was then demonstrated to interact strongly with malachite green and lead ions (Pb^{2+}) in water. Adsorption efficiencies of 20.7 and 21.05 mg·g^{-1} were reported for malachite green and Pb^{2+}, respectively. These adsorbed contaminants were desorbed repeatedly using ethanol and EDTA to elute the contaminant and the modified nanoparticles reused. After six cycles the remaining removal efficiency for malachite green and Pb^{2+} was 56% and 61.5%, respectively. The modification of magnetic Fe_3O_4 nanoparticles with the amino acid *L*-cysteine through postsynthetic modification was reported by Bao et el. [55] who observed that these particles aggregated in the presence of sodium alginate into beads (millimeter-sized) that can adsorb Pb^{2+} ions from water with a maximum adsorption of 310.03 mg·g^{-1}.

Polythiophene was bound to the surface of copper ferrite ($CuFe_2O_4$) nanoparticles (size range 11–30 nm) by Al Omar et al. [56] who then tested these nanoparticles for the removal of mercury ions (Hg^{2+}) from water. The modification of these nanoparticles greatly increased the level of adsorption compared to unmodified nanoparticles with the values going from 7.53 to 208.77 mg·g^{-1}. The particles were reused up to five times with moderate reduction in removal efficiency. It was observed the Hg^{2+} ions were bound both to the polymer sheath and directly to the surface of the nanoparticles through oxygen and sulfur containing groups.

Polyethylenimine was used to stabilize spherical magnetic iron (Fe_3O_4) particles (average size, 10 nm) by Kim et al. [57] who then demonstrated the ability of these nanomaterials to connect to and remove clay particles from a soil suspension. The clay particles examined in this case demonstrated a strong efficiency for radioactive cesium (^{137}Cs) ions. As such, this may be an important method for the removal of radionucleotides from contaminated soils.

Silane based thiols were bound to the surface of magnetite (average size, 20 nm) by Canepa et al. [58] who then tested this material for the quick removal of Pb^{2+} from water. When examined for the removal of Pb^{2+} from a defined water source the functionalized nanoparticles were reported to extract 91% within 10 min. Repeated cycles of extraction and desorption of Pb^{2+} ions were carried out and showed a drop in extraction efficiency over each cycle with just over 34% on the fifth cycle. When these nanoparticles were placed into a dynamic circuit it was reported that only around 21% of available Pb^{2+} was extracted. This is suggested to be due to the relatively weak interaction between the metal ion and the thiol group which will permit the ion to be decoupled by the flow of the liquid. Novel designs for the liquid flow are suggested as a possible solution to this problem.

Another form of surface modification was reported by Zhang et al. [39] who generated hollow spheres of magnetic carbon through a hydrothermal synthesis. These spheres (average size ~400 nm) were then functionalized with carboxylic acid groups and tested for the removal of Pb^{2+} ions from solution. They achieved a maximum adsorbance capacity of 179.21 $mg{\cdot}g^{-1}$ at pH 7. This form of particle was investigated as a potential method to immobilize free Pb^{2+} ions in soil water.

2.3. Metal Ferrite Magnetic Nanoparticles

The following are a selection of reports of ferrite nanoparticles. By changing the synthesis conditions used in their formation, investigators were able to generate a many different nanomaterials with properties with potential applications in the remediation of water.

Cobalt and manganese ferrite ($CoFe_2O_4$ and $MnFe_2O_4$) nanoparticles were generated and their adsorbance properties compared to that of regular iron ferrite (Fe_3O_4) by Trindade et al. [59]. The resulting nanoparticles had averages sizes of 30, 75 and 60 nm for $CoFe_2O_4$, $MnFe_2O_4$ and Fe_3O_4, respectively. While it was reported that in all cases these nanoparticles can remove sufficient As(V) from water to reduce its level to that deemed safe by the World Health Organization, they found that the ferrites functioned to remove more arsenic ions from water than iron ferrite. However, they also released cobalt and manganese cations into water when in suspension. Gaps in the structure made by the release of the cations gave space for As(V) ions from the solution. This issue with leaching of cations makes the point that the design of an appropriate nanosorbent for arsenic will not be selected by solely seeking the sorbent with the highest maximum adsorption capacity.

Cobalt ferrite (average size, 10–20 nm) was examined by Dionysiou et al. [60] for the activation of PMS for the degradation of bisphenol A in water as well as other recalcitrant organic contaminants. This catalytic system demonstrated successful operation in both controlled water conditions and in water taken from the environment. The addition of anions like hydrocarbonate (HCO_3^-) and chloride (Cl^-) enhanced the degradation as did the addition of humic acid up to 10 $mg{\cdot}L^{-1}$, but fulvic acid had a negative effect at a concentration higher than 1 $mg{\cdot}L^{-1}$. An interesting mixed ferrite was reported by Liu et al. [40] where a nickel, magnesium and zinc, ferrite ($Ni_xMg_yZn_{(1-x-y)}Fe_2O_4$) was synthesized by an ethanol mediated combustion process. After calcination at 400 °C these particles (average size, 27.5 nm) were reported to be able to adsorb methylene blue to a maximum capacity (q_{max}) of 1654.55 $mg{\cdot}g^{-1}$. This high value was determined to be the result of the presence of multimolecular stacking of dye molecules on the surface of the particles. The nature of adsorption binding was also confirmed through the use of electrochemical analysis which determined a higher degree of resistance with the adsorption of methylene blue which would be indicative of the formation of an organic layer over the particle surface. This high degree of adsorption was reported for pH ≥ 5 and was reported to be reduced to less than 3% after the first three cycles of extraction.

Magnesium ferrite ($MgFe_2O_4$) (average size, 120 nm) formed through an alcohol-based combustion process was also reported by Wang et al. [61] for the removal of reactive red. A maximum adsorption capacity of 119.1 $mg{\cdot}g^{-1}$ was reported and electrochemical analysis by cyclic voltammetry demonstrates that the dye molecules form a monolayer, occupying all active sites.

Another similar magnetic multi metal oxide material was reported by Ahmad et al. [41] who made zinc, manganese, iron mixed metal nano oxide ($Mn_xZn_{(1-x)}Fe_2O_4$) nanoparticles. Size and morphologic data were not provided for these materials. These were tested for catalyzing the Fenton reaction for the degradation of reactive yellow 15 dye from water. When the pH was set at 4 and the nanocomposite raised up to 1 $g{\cdot}L^{-1}$ up to 76% of the dye was degraded.

A copper modified magnetic iron oxide (Cu–nFe_3O_4) (size range, 15–20 nm) was reported by Zou et al. [42] who then tested this nanomaterial for the degradation of the antibiotic chlorotetracycline. It was observed that this nanocatalysts can degrade up to 99% of a 100 $mg{\cdot}L^{-1}$ solution of chlorotetracycline in the presence of a 2 $g{\cdot}L^{-1}$ suspension of the nanocatalyst over 90 min. The nanocatalyst performed well over multiple cycles of the degradation of the contaminant. It was also reported that the presence of phosphate greatly inhibited the reaction while other ions did not and that humic acid can either promote or inhibit the reaction depending on its concentration. An examination of the reaction mechanism indicates that contaminant is physiosorbed on the surface and pores of the particles and then reacts with Fe(II) and Fe(III) ions forming radical species of the contaminant and oxygen which then degrades the organic contaminant.

Surface oxygen vacancies were induced in hexagonal cobalt zinc ferrite ($ZnFe_{0.8}Co_{0.4}O_{2.4}$) (size range 20–60 nm) by Hu et al. [43] through a sol–gel combustion method and where then used to induce activation of PMS to generate reactive oxygen species for the degradation of organic pollutants such as bisphenol A and diphenhydramine. This nanocatalyst showed strong activity with complete degradation of 10 $mg{\cdot}L^{-1}$ solutions of the organic pollutants in as little as 4 min. Cui et al. [62] reported a similar structure of copper substituted zinc ferrite (irregular shape, size range, 10–100 nm). This material too demonstrated improved catalytic activation of PMS and when tested against the antibiotic ciprofloxacin, demonstrated over 96% degradation in 15 min.

The catalytic activity of cobalt ferrite ($CoFe_2O_4$) nanoparticles (average size 36 nm) for the activation of PMS with the aim of degrading organic contaminants in water was investigated by Chang et al. [63] who introduced the reductant hydroxylamine to reduce Co and Fe ions to keep the redox cycles active and stabilize some of the radical species. For this reason, the presence of hydroxylamine leads to excellent catalytic behavior for the degradation of the antibiotic sulfamethoxazole, showing complete degradation in approximately two hours. When tested for activity in groundwater samples, the nanoparticle/hydroxylamine mixture still shows good activity after 6 cycles.

Iron manganite ($FeMnO_3$) nanoparticles were synthesized by Nikolic et al. [44] using a sol–gel combustion process with glycine as a fuel. The resulting particles had a porous plate-like stricture with a mean size of around 180 nm. These nanoparticles were then tested for inhibitory effects on the soil bacterium *Bacillus subtilis*. The nanoparticles showed around 50% inhibition of bacterial growth when in Luria–Bertani (LB) medium but had no effect when in brain heart infusion (BHI) medium. It is believed that the rich concentration of proteins and oligosaccharides in BHI passivated the surface of the nanoparticles while this does not occur in LB as a larger concentration of free Mn ions was observed in it.

Bakshi et al. [64] reports an interesting method for the removal of Au and Ag nanoparticles from water solution through the addition of magnetic iron oxide nanoparticles (average size ~20 nm) which have been synthesized in the presence of a gemini surfactant, namely a long-chained amino ion through a solvothermal synthesis. It was observed that these surfactants can form an amphiphilic structure which can serve to draw metallic nanoparticles of different surface polarities away from free media to an organic/water interface, enabling removal with a magnet.

An interesting photocatalytic nanoparticle was reported by Ashour et al. [45] who synthesized magnesium-doped manganese zinc ferrite (spherical morphology, average size, 30 nm) through a step wise process whereby a selected ratio of nitrate salts of the four metals were mixed with citric acid and ethylene glycol to from a gel. After drying at 120 °C, grinding and sintering at 900 °C the resulting $Mn_{0.5}Zn_{0.5-x}Mg_xFe_2O_4$ powder was tested for photocatalytic activity under UV light (254 nm). It was observed that where x is equal to 0.375 the photocatalytic activity was the highest with 95% degradation

of rhodamine B and 90% of chloramine at pH 11 after 80 min of UV irradiation. This activity was reported to still be retained after several cycles. The nanoparticles were also reported to demonstrate antibiofilm activity with the highest degree of inhibition reported for *Pseudomonas aeruginosa* with more than 98% inhibition for where x is equal to 0.25. This material was tested for antimicrobial activity. After 60 min under UV irradiation there was a marked reduction in microbial activity. The bacteria, *Pseudomonas aeruginosa* demonstrated over 90% inhibition, the other bacteria *Staphylococcus aureus* showed more than 65% and the fungi *Candida tropicalis* presented more than 88% inhibition.

Antibacterial activity was also reported by El Nahwary et al. [46] who demonstrated antibacterial activity of cubic nanoparticles of $Ni_{0.6}Zn_{0.4}Fe_2O_4$ and $Ni_{0.6}Zn_{0.2}Ce_{0.2}Fe_2O_4$ which were generated by sol–gel treatment with citric acid followed by calcination at 700 °C. These nanoparticles, (size range 30–35 nm) greatly inhibited microbe growth under laboratory conditions with reductions reported in the growth of the bacteria *P. aeruginosa* and *S. aureus* and the fungi *C. albicans* and *Aspergillus niger*. All showed substantial reduction in microbial survival with increasing exposure time with full inhibition of all types of microbe after 30 min exposure to 200 $mg{\cdot}L^{-1}$ of the nanoparticles. It was also reported that there was a marked increase in inhibition rates for all microbe classes with the cubes containing cerium. This was postulated to be due to the presence of Ce^{3+} associated with ferrite which had already been exhibited as an affective antimicrobial agent. Finally, the nanoparticles were tested against raw sewage samples taken from a municipal drain. Untreated samples were confirmed to contain a number of potentially pathogenic species such as *Escherichia coli*, *Salmonella enterica*, *S. aureus* and *Listeria monocytogenes*. In all cases the presence of a dose of these cubic nanoparticles of 150 $mg{\cdot}L^{-1}$ reduced the number of colony-forming units by a factor of approximately 6-log_{10}. The authors of the study reported that these nanoparticles may be a useful tool for the removal of pathogenic microbes from wastewater before release into the environment.

2.4. Zerovalent Iron Nanoparticles

While chemically simple, consisting of pure iron, these particles show interesting chemical and physical properties which make them very suitable for use as agents for the removal of many different contaminant species. In several of the following cases zerovalent iron was presented with an average particle diameter greatly more than 100 nm. This may be traced to the synthesis method used for the generation of these particles (ball-milling of fine powders). In such cases it may be noted that they still retain a magnetic response (though would not be superparamagnetic) and catalytic behavior sufficiently similar to that of nanoscale nZVI particles that they may be justified in their inclusion in this review.

A very interesting potential application for nZVIs was described by Zhang et al. [47] who examined the efficacy of such nanoparticles for the pretreatment of wastewater before their processing in bioreactors. It was reported that zero-valent iron nanoparticles (average size, ~40 nm), generated through a sodium borohydride reduction, could reduce the water-soluble dye molecule Congo red into waste products which could then be readily consumed by bacteria in membrane bioreactors. Even after 52 days of use, up to 99% reduction in dye concentration and over 50% reduction in the chemical oxygen demand of simulated wastewater was achieved.

Sun et al. [65] also reports the application of polyvinylpyrrolidone (PVP) stabilized spherical nZVIs (size range, 50–80 nm) for the removal of trichloroethylene from soil. When cetyltrimethylammonium bromide (CTAB) or sodium dodecyl sulfate (SDS) was applied with the nanoparticles there was an increase in the transfer for the organic contaminant to the liquid phase and a consequent increase in reductive dichlorination. Close to 100% of the trichloroethylene in a soil sample was removed by the nanoparticle_SDS pairing. As such surfactants may be a valuable tool for assisting other nanocatalysts in the future.

The use of sulfur modified nZVIs (S–nZVIs) was reported by Sun et al. [48] and by Ren et al. [66] for the catalytic activation of peroxydisulfate which can then be used for the breakdown of organic pollutants. Sun used the drug molecule acetaminophen and Ren the antibiotic sulfadiazine as examples for degradation targets with acetaminophen showing a maximum of just over 5 times increase in the rate of removal and sulfadiazine showing more than twice the rate of degradation compared to unmodified nZVIs. It was reported by Sun that while the S–nZVIs demonstrated higher degradation rates in the presence of oxygen, there was a further increase in the rate for both in the absence of oxygen, an effect which indicates that while oxygen can increase the available catalytic iron ions, it also can compete with the peroxydisulfate for those same species. Ren studied the effect of other ions in the reaction medium. They reported that the presence of SO_4^{2-} and Cl^- can lead to a decrease in the level of enhancement by sulfurization and that NO_3^- can increase it.

The modification of nZVIs with carbon through a ball milling process was also investigated by Sun et al. [49] who tested these new materials for removal of trichloroethylene. It was observed that the rate of degradation of the organic contaminant had increased greatly, but also that the fastest reaction was achieved with a small weight percentage of carbon though this then affected the stability of the resulting particles. The thicker carbon coatings did not exhibit as much of an enhancement, but this could be ameliorated by using carbon with improved electron transport ability (carbon fiber as opposed to activated carbon).

The synergistic interactions between more than one contaminant was reported by Chen et al. [67] who investigated the adsorption of uranium U(VI) and phosphate (PO_4^{3-}) on nZVIs (size range, 10–100 nm). When used together, the adsorption capacity of U(VI) and PO_4^{3-} increased by over 20% and 30%, respectively. As multiple ions are usually present in real water sources, this effect may have real application in the use of this technology. Similar synergistic effects were observed for S–nZVIs (mean size, 240 nm) in the presence of both Pb^{2+} and polybrominated diphenyl ether by Dang et al. [68] where it was reported that the rate constants of removal of both Pb^{2+} and the ether increased by 5.15 and 7.29 times, respectively. It was observed that the lead ions were adsorbed onto the surface of the nanoparticles and converted into immobilized lead species. These surface lead ions then aided the reductive degradation of polybrominated diphenyl ether. However, the overall stability of the resulting particles is reduced as the Pb^{2+} ions accelerates their corrosion.

A mixture of theoretical and experimental studies of the mechanism for the binding of metal ions to the surface of nanoparticles was conducted by Bhateria et al. [50] who looked at the adsorbance of lead ions onto magnetite needle-shaped nanoparticles (average length, 100 nm). They found that the adsorption process was highly pH dependent and that it obeyed the Langmuir isotherm which would indicate the formation of a monolayer of Pb^{2+} ions on the nanoparticle surface. It was observed that the adsorption process can be reversed readily with a small loss of function and that the nanomaterials which have been generated specifically for the study demonstrated good levels of adsorbance (41.1 $mg{\cdot}g^{-1}$). They also note that the maximum level of adsorbance is favored in scenarios where the nanoadsorbent is in lower concentration and that at higher concentrations the magnetic nanoparticles tend to aggregate reducing the available surface area. This effect may be reduced through the addition of stabilizers or other coatings, but such a modification may influence the adsorption properties of the nanomaterial.

The effect of the presence of other environmental polyelectrolytes on the adsorption of phosphate (PO_4^{3-}) on to ZVIs (size range, 30–300 nm) was investigated by Shanableh et al. [69] who investigated changes in the adsorption in the presence of humic acid and chitosan. It was found that at low pH the maximum adsorbance for free particles (523 $mg{\cdot}g^{-1}$) decreased in the presence of chitosan to 342 $mg{\cdot}g^{-1}$ but increased with humic Acid to 697 $mg{\cdot}g^{-1}$. However, when pH increased to 6.5 the value for free nanoparticles (412 $mg{\cdot}g^{-1}$) was enhanced up to a maximum of 790 $mg{\cdot}g^{-1}$. It is suggested that the charged organic polymers can influence the interactions necessary for the adsorption of phosphate such as electrostatic adsorption, ion exchange and precipitation and that pH can also strongly influence these effects. As many environmental samples would contain dissolved organic

matter of a composition similar to these polyelectrolytes it is likely that these effects will need to be considered for the application of such technology in the field. A similar effect on the adsorption of heavy metals was observed by Lou et al. [70] who tested the effect of the presence of other ions in the solution such as nitrate (NO_3^-) chloride (Cl^-) and humic acid on copper (Cu^{2+}) and nickel (Ni^{2+}) adsorption on S-ZVIs particles (size range, 100–200 nm). While it was observed that the adsorption capacity of the S-ZVIs was good for the heavy metals, the presence of ions affected the adsorption of Cu^{2+} but had very limited effect on Ni^{2+}. This could be due to the Cu^{2+} being retained by reduction and adsorption while Ni^{2+} retention occurred primarily through the latter process. A possible method to reduce the effect of humic acid was reported by Guan et al. [71] who observed that while large concentrations of humic acid can inhibit ZVI particle (D_{50} 108 μm) reduction of nitrophenol, the addition of an excess of Fe^{2+} can mitigate this inhibition. They surmise that the Fe^{2+} can both aid the formation of an oxide structure on the particle surface that can mediate the reduction of the nitrophenol and can aggregate the humic acid preventing it from occupying sites for nitrophenol reduction.

Non-chemical environmental effects were also shown to be important. It was observed by Guan et al. [72] that a weak magnetic field can increase the adsorption selectivity for the metalloid oxyanions As(III), As(V), Sb(III), Sb(V), Se(IV) and Se(VI) for ZVIs. It was reported that the selectivity for the metalloid ion Se(IV)/Se(VI) increased by as much as 14 times compared to particles with no field. It was reported that while the electron utilization (the number of electrons expended in reaction) was the same regardless of the presence of a magnetic field, the field did alter the electron efficiency (the percentage of electrons that reduced a specific target) and that this effect may be due to the movement of free Fe^{2+} ions around the nanoparticle with the target metalloid oxyanion in tow.

Guan et al. [73] also observed that the addition of Fe^{2+} to the solution, the addition of H_2O_2, the sulfurization, or the application of a weak magnetic field to ZVI particles can increase the rate of removal of selenium (VI) with the addition of Fe^{2+} showing the most pronounced effect.

2.5. Conclusions

In conclusion, the latest developments on single magnetic nanoparticle materials show they have excellent potential as agents for the remediation of water. First, the development of magnetic nanoparticles with different morphologies was reported, from rings to tubes. These reports included many different processes for contaminant removal ranging from adsorption to photocatalysis. Surface modification followed with examples of simple organic species like silane thiols up to carbon coating. The reports solely included adsorption behavior in this case. The ferrite nanoparticles listed in the third section were observed engaged in many different contaminant removal processes from adsorption to photocatalyst. Through modification of the chemical make-up of the ferrite different reactivities could be achieved. Finally, zerovalent iron particles (nZVIs) demonstrated good efficiency as adsorbents and catalysts. Though uncoated nZVIs were observed to easily corrode, coating them with sulfur or carbon promoted greater stability. The observed need for passivation of nZVIs would make them an interesting component of composite materials as would be discussed in the next two sections.

3. Magnetic Nanocomposites

There are a number of materials which use more than one nanomaterial in the same composite so that the different properties of these nanomaterials work together to achieve the desired material performance. These materials are termed nanocomposites; composites containing magnetic nanomaterials were examined as potential agents for the remediation of water. In the following section different magnetic nanocomposites are listed.

3.1. Clay/Magnetic Nanoparticle Composite Materials

Various magnetic nanocomposites generated using either naturally occurring or synthetic clays and similar minerals have been reported for the adsorption (Table 3) and catalytic conversion (Table 4) of contaminants in water.

Table 3. Selected examples of adsorbent composites of clay-like materials and magnetic nanoparticles as adsorbents.

Core Magnetic Nanoparticle (MNP)	Mineral Coating	Surface Area (m^2 g^{-1})	Contaminant	Q_{max} ($mg \cdot g^{-1}$)	Ref
$CoFe_2O_4$	Cu/Al LDO/LDO	89 (17.6 calcined)	Methyl orange	1355.1	[74]
Fe_3O_4	Ni/Fe LDH	93.9	Histidine	3287.67	[75]
Fe_2O_3	Sericite Clay	161.5	Methylene blue crystal violet	35.36 35.45	[76]
Various iron oxides	Spent bleaching earth	122.1	Tetracycline	106	[77]
$ZnFe_2O_4$	Hydroxyapatite	60.2	Cd^{2+}	120.33	[78]

Layered double hydroxides (LDH) and their calcined counterparts layered double oxides (LDO) have been demonstrated as an interesting nanomaterial for the removal of contaminants from water [79]. While it has already been reported that high adsorption values can be achieved for composite nanomaterials consisting of layered double oxides with magnetic nanoparticles [80] a quite interesting observation was made by Palza et al. [74] that when the concentration of nanoparticles to LDH nanosheets were altered there was also a strong effect on the adsorption capacity of composite. It was observed that out of three different ratios of cobalt ferrite ($CoFe_2O_4$) nanoparticles (average size, 11 nm) to Cu/Al layered double hydroxide the ratio with the lower concentration of magnetic nanoparticles resulted in higher adsorbance of methyl orange from water (262 $mg \cdot g^{-1}$) than for the composite with the higher concentration of magnetic nanoparticles (136.2 $mg \cdot g^{-1}$). With calcination at 500 °C for four hours these adsorbance values were increased to the incredibly high 1355.1 $mg \cdot g^{-1}$ for the composite with the lowest concentration of magnetic nanoparticles and an observed doubling in the composite with highest concentration up to (304.9 $mg \cdot g^{-1}$). It is theorized in the report that there is a sweet spot were higher than unity levels of adsorbance can be achieved due to disruption of the laminar structure of the LDH, but before the nanoparticles block available sites for binding by dye molecules. While the nanocomposite showed a reduced magnetic response with lower $CoFe_2O_4$ concentration, it was still sufficient to withdraw the composite from suspension with application of a permanent magnet.

This above unity adsorbance has not only been reported for dye molecules. When bound to magnetite nanoparticles by Wang et al. [75] through a process involving a Fe_3O_4 core (average diameter, 400 nm) onto which was bound MOF mediated in situ cascade derivation strategy (Figure 2). The resulting nickel/iron LDH shows strong affinity for histidine rich protein molecules due to the large quantity of nickel atoms on its surface. It was that when presented with bovine hemoglobin, a Histidine rich protein, very high levels can be adsorbed (3287.67 $mg \cdot g^{-1}$ at pH 7). This indicates good potential for use in situations with the need for selective adsorbance of biologic molecules.

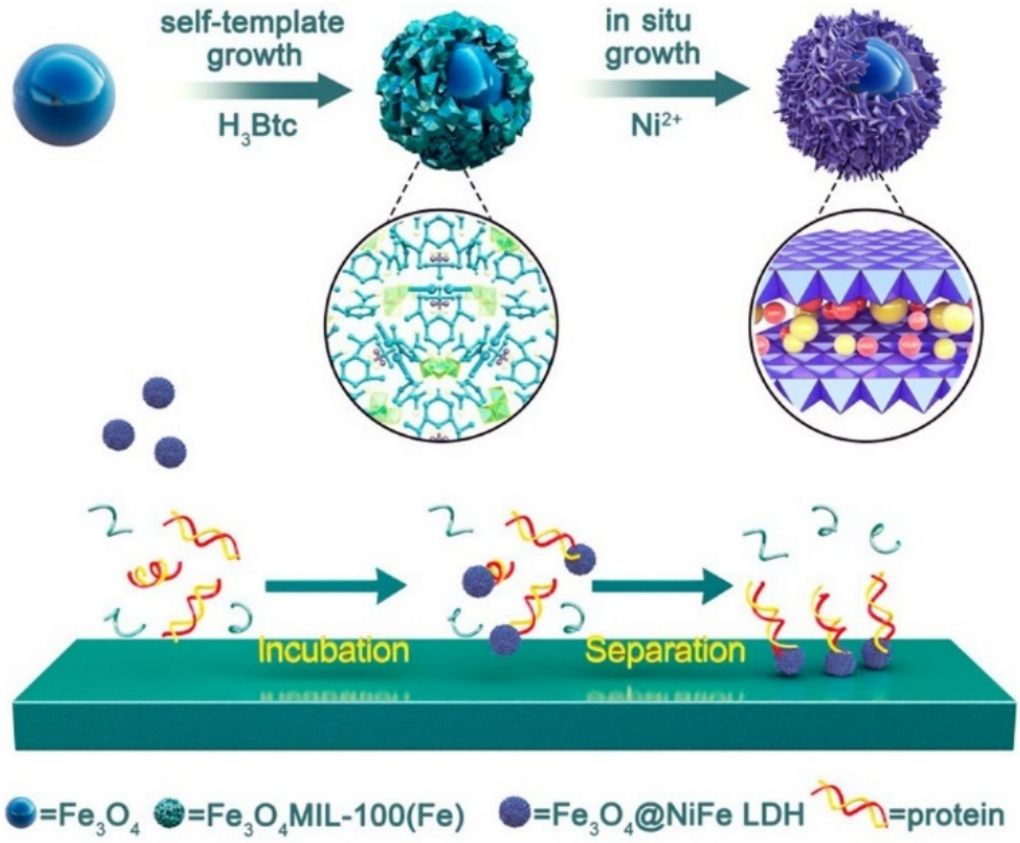

Figure 2. Proposed scheme for the synthesis of nickel/iron layered double hydroxides (LDH) through the use of an in situ cascade derivation strategy. Reprinted with permission from Wang et al. [75] Copyright 2020 American Chemical Society.

A magnetic layered double hydroxide waste sludge activated carbon derived (average size, 30 nm) from water treatment was used as the base for the synthesis of Mg–Fe layered double hydroxide by Quereshi et al. [81] using a basic reflux. The resulting composites demonstrated a good magnetic response and were observed to adsorb NO_3^{2-} and PO_4^{3-} with maximum adsorption coefficients of around 54.5 and 110 mg·g^{-1}, respectively.

Similar to LDHs, inorganic clays also provide an interesting opportunity for the removal of contaminants from water. With the binding of Fe_2O_3 nanoparticles (size range, 4–8 nm) to sericite clays Abdullah et al. [76] was able to develop a composite system which was able to adsorb both methylene blue and crystal violet from water. Adsorption capacity values of 35.36 and 35.45 mg·g^{-1} was reported for methylene blue and crystal violet, respectively. When crystal violet dye was removed from the composite through elution with an acetic acid/ethanol mixture with sonication the composite was reused. There was found to be a slight reduction in the removal efficiency after each cycle with only 70% removal reported after the 5th cycle.

Another inorganic clay material which can be utilized for the removal of contaminants would be spent bleaching earth. As reported by Wan et al. [77] used bleaching earth, which is a clay material used for the removal of contaminants from edible oils, was taken and functionalized with magnetic iron oxides. They took used bleaching earth, pyrolyzed it at 700 °C and then grew iron oxides nanoparticles on the surface of earth particles using a co-precipitation method. This composite material showed a strong adsorbance of the antibiotic tetracycline demonstrating a maximum adsorbance capacity (Q_0) of 0.238 mmol·g^{-1} even higher than that reported for spent bleaching earth that has not been functionalized (Q_0 = 0.150 mmol·g^{-1}). With the examination of the potential reuse of this composite it was observed that the level of removal of tetracycline dropped down in the first two cycle followed

by it leveling off for the remaining three cycles. The authors indicate that this level of removal may continue unreduced for up to 8 more cycles.

Table 4. Magnetic nanocomposites functionalized with minerals which were reported to have catalytic activity against contaminants.

Core NMP	Clay Component	Surface Area (m^2 g^{-1})	Contaminant	Method of Removal	Ref
Fe_3O_4	Attapulgite/CuO/CeO_2	150.8	Methylene blue	Fenton catalysis	[82]
S–nZVIs	Montmorillonite	N/A	Trichloroethylene	Reduction	[83]
Fe_3O_4	Schwertmannite	59.7	Ciprofloxacin	Fenton reaction	[84]
$CoFe_2O_4$	Diatomite	137.8	Bisphenol A	PMS activation	[85]
$CoMn_2O_4$	Fibrous phosphosilicate	124	4-nitrophenol 2-nitroaniline	Catalytic reduction	[86]
Fe_2O_3	Zeolite	264	Methylene blue	Fenton reaction	[87]
Fe_3O_4	Halloysite ZnO	N/A	Various bacteria	Inhibition of growth	[88]

The use of another clay was reported by Wang et al. [82] who synthesized iron oxides nanoparticles (Fe_3O_4) (size range, 10–50 nm) in conjunction with either copper oxide (CuO), Cerium oxide (CeO_2) or a mixture of the two on a base of attapulgite clay. These nanocomposites were tested as Fenton Catalysts for the degradation of the organic dye, methylene blue. It was found that the catalytic activity of the magnetic clay catalysts was enhanced by the presence of the additional dopants and that a high degree of dye degradation (>99% of a 100 $g{\cdot}L^{-1}$ solution in all cases) of methylene blue was achieved at pH 5. The catalysts were reused with a high degree of degradation of methylene blue up to three times. It was also reported that the intermediate degradation products for the methylene blue were determined to be mainly benzoquinone, hydroquinone, catechol and resorcinol which indicates a reaction mechanism operating through radical attack against the -S= and -N= bonds.

The mineral montmorillonite was used by Jiang et al. [83] as a scaffold for the synthesis of S–nZVIs (average size, ~1 nm). The layered structure served two purposes, it protected the nanoparticles from corrosion and it prevented interference in catalytic activity by polyelectrolytes such as humic acid. The montmorillonite supported S–nZVI composites also demonstrated favorable activity for the catalytic reduction of trichloroethylene with reported degradation values for a 250 $mg{\cdot}L^{-1}$ solution of more than 78% after 12 h, far higher than that reported for free S–nZVI or non-sulphurated nZVI in montmorillonite.

The mineral schwertmannite was modified with magnetic Fe_3O_4 nanoparticles (average size, 10 nm) by Zhou et al. [84] and tested as a Fenton catalyst for the degradation of organic contaminants. When tested against the antibiotic ciprofloxacin, this composite demonstrated close to 97% removal of a 50 $mg{\cdot}L^{-1}$ solution over 6 min in an excess of H_2O_2. This level of activity continued with negligible change for 4 cycles of use. Similar results were reported for the other model organic contaminants of phenol, tetracycline, acid orange 7 and methylene blue.

Diatomite is another mineral used by Zheng et al. [85] as a support for the synthesis of cobalt ferrite nanoparticles (average size, 5 nm) through a citrate combustion method. These nanocomposites were used in conjunction with PMS for the degradation of bisphenol A. Compared to the two components as separate materials, the diatomite/cobalt ferrite composite exhibited very strong catalytic activity and 100% of a 25 ppm bisphenol A solution was degraded (Figure 3).

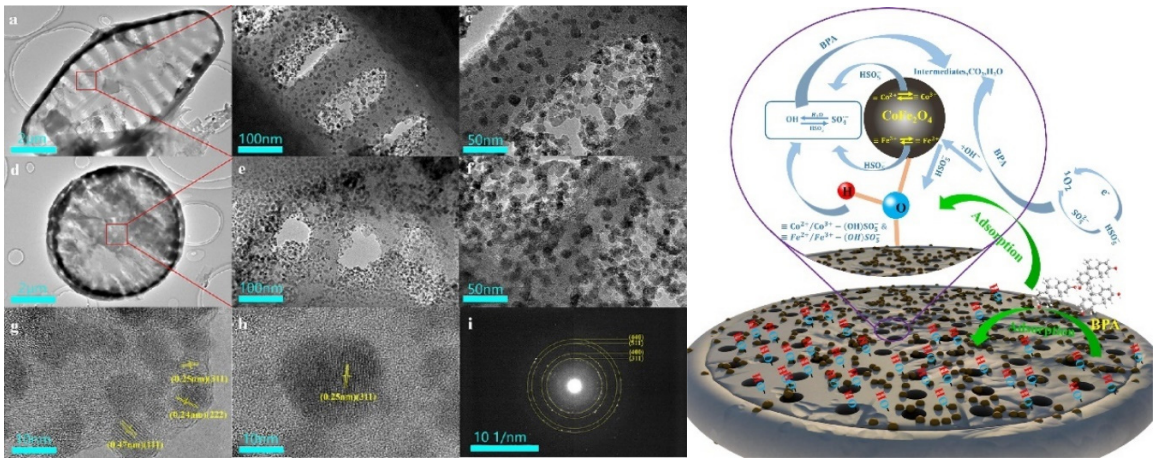

Figure 3. Images of (**left**) TEM micrographs of diatomite particles on to which $CoFe_2O_4$ nanoparticles were placed and (**right**) a proposed mechanism scheme for the conversion of PMS into reactive oxygen species for the degradation of bisphenol A. Reprinted from Zhang et al. [85] with permission from Elsevier.

A catalytic composite of fibrous phosphosilicate nanoparticles was used by Sadeghzadeh et al. [86] who then coated such particles with octakis[3-(3-aminopropyltriethoxysilane)-propyl] octasilsesquioxane and then magnetic cobalt manganate ($CoMn_2O_4$) nanoparticles (average size, 10 nm) were grown on this surface to create microspheres. These nanocomposites were tested for the reduction of the organic contaminants 4-nitrophenol and 2-nitroanaline. The percentage conversion of 4-nitrophenol was reported to be close to 99.8% of a 0.0126 M solution in 100 s. The rate of this reaction was determined and was found to compare well to other nano-catalysts [89–92]. The catalyst was reused up to ten times without a large drop in activity.

The use of the mineral hydroxyapatite, formed around $ZnFe_2O_4$ magnetic nanoparticles (average size, 28 nm) was reported by Dhar et al. [78] who investigated this composite for the removal of Cd^{2+} from water. The composite demonstrated good adsorption with a reported maximum adsorption capacity of 120.33 $mg{\cdot}g^{-1}$. The authors have proposed that the adsorption occurs through an ion replacement process where calcium ions in the mineral are replaced with cadmium ions. However, he desorption of cadmium from the nanocomposite was not demonstrated by the authors. This possibly means more nanocomposite would be required than would be necessary for a reversible process.

Zeolite formed from fly ash derived from lignite combustion was used by Václaviková et al. [87] in a fusion hydrothermal process to add in various types of nanomaterials including magnetic hematite (average size, 10 nm) which formed a magnetic composite. They demonstrated a high surface area of 264 $m^2\ g^{-1}$ though somewhat reduced compared to pure zeolite of 486 $m^2\ g^{-1}$ and showed good adsorption of Cd^{2+} and Pb^{2+} ions from water (163.7 $mg{\cdot}g^{-1}$ for Cd^{2+}). They were also demonstrated as Fenton catalysts, aiding in the degradation of methylene blue dye with higher activity being reported for the modified zeolite at lower temperature due to distortion of the structure due to the presence of the magnetic particles.

Inorganic nanotubes made of halloysite were coated in Fe_3O_4 and ZnO nanostructures (size range, 5–6 nm) by Kadam et al. [88] which were then tested for antibacterial activity. These composites demonstrated strong inhibitory effects against *E. coli*, *S. aureus* and *MRSA*. However, while the nanocomposite can inhibit the formation of biofilms for *E. coli* and *S. aureus*, it does not inhibit the formation of biofilms in *MRSA*.

3.2. Carbon/Magnetic Nanomaterial-Based Nanocomposites

Carbon nanomaterials have been viewed as a very interesting potential material for the generation of novel nanocomposites due to both the availability of the starting material and their interesting properties (Table 5). An interested effect was reported by Yamaguchi et al. [93] who reported the synthesis of a composite of manganese ferrite ($MnFe_2O_4$) particles (average size, 200 nm) supported by graphene oxide and sand through a solvothermal process. These composites with particles of approximately 200 nm in size demonstrated effective degradation of methylene blue in the presence of light and H_2O_2 through the Fenton reaction. A similar, but simpler system was reported by Gaspar et al. [94] who synthesized magnetite (average size, 21 nm) with reduced graphene oxide (Fe_3O_4/RGO). With the magnetite in large excess (approximately 90% per weight) this nanocomposite exhibited a strong catalytic activity for the Fenton reaction in water at pH 6. When tested against indigo carmine this catalyst was able to achieve 100% discoloration within only 5 min. This material was also strongly magnetic and as such was readily removed from suspension and was also readily reused at least once according to reports.

Table 5. Magnetic nanocomposites with carbon species for removal of contaminants.

Core NMP	Form of Carbon or Additional Material	Surface Area (m^2 g^{-1})	Contaminant	Method of Removal	Ref
$MnFe_2O_4$	Graphene oxide + sand	N/A	Methylene blue	Fenton reaction	[93]
Fe_3O_4	Reduced graphene oxide	177	Indigo carmine	Fenton reaction	[94]
γ-Fe_2O_3	Graphene oxide	177	17β-estradiol 17α-ethinylestradiol	adsorption	[95]
Fe_3O_4	Graphene oxide + SiO_2	N/A	Cd^{2+} + Pb^{2+}	adsorption	[96]
Fe_3O_4	Graphene oxide aerogel	157	Rhodamine B, methyl orange methylene blue	Photocatalytic oxidation	[97]
$CoFe_2O_4$	Graphene oxide aerogel	341.6	Benzotriazole	PMS activation	[98]
Fe_3O_4	Reduced graphene oxide polypyrrole	33	Pb^{2+}	Adsorption	[99]
$ZnFe_2O_4$	Reduced graphene oxide tio_2 nanosheets	N/A	p-nitrophenol	Photocatalytic oxidation	[100]
Fe_3O_4	S and n-doped graphene oxide with *l*-cysteine	96.3	Methylene blue, Congo red and neutral red	Adsorption	[101]
Fe_3O_4	Graphite poly polyethyleneimine	12.8	Humic acid	Adsorption	[102]
$Co_{0.5}$ $M_{0.5}$ Fe_2O_4	Carbon nanotubes	112	Pentachlorophenol	Adsorption	[103]
Fe_3O_4	Carbon nanotubes	N/A	*Microcystis aeruginosa*	Agglutination	[104]
Fe	Carbon nanotubes Cu, CuO, Al	111.3	Sulfamerazine	Oxygen reduction, Fenton reaction	[105]
$Fe_{20}Cu_{80}$	Nanodiamond	N/A	Phenol	Fenton reaction	[106]
Ni_nFe	Activated carbon	N/A	Perfluorooctanesulfonate	Reduction	[107]
nZVIs	Carbon black	619.8	Chloramphenicol	Adsorption + reduction	[108]

Graphene oxide was also bound to γ-Fe_2O_3 magnetic nanoparticles (average size, 11 nm) through a simple co-precipitation reaction by Santos De Gois et al. [95] These nanocomposites were used to concentrate 17β-estradiol and 17α-ethinylestradiol. for further analysis. These two chemicals are both estrogen mimics which have been linked with environmental effects against aquatic life and may be harmful to humans if found in drinking water. Graphene oxide in conjunction with silica coated magnetite particles (Fe_3O_4/SiO_2–GO) (average diameter, 220 nm) was reported by Sun et al. [96] who demonstrated this material's effectiveness for the removal of Cd^{2+} and Pb^{2+} from water. They report maximum adsorption capacities of 128.2 and 385.1 mg·g^{-1} for Cd^{2+} and Pb^{2+}, respectively. After sonication aided acid desorption of the adsorbed contaminants, the composite still demonstrated good performance even after 12 adsorption/desorption cycles.

Graphene oxide was also utilized as a basis for the formation of an aerogel by Ge et al. [97] who then investigated this material as catalysts for the degradation of rhodamine B, methyl orange and methylene blue. The generation of the aerogel involved the synthesis of 10 nm magnetite nanoparticles. When irradiated with visible light the quantity of methylene blue dye was reduced by close to 98% within 180 min. Graphene oxide was also formed into an aerogel with $CoFe_2O_4$ nanoparticles (average size, 10 nm) and-doped with nitrogen by Lyu et al. [98] who then tested this aerogel by for the oxidation of benzotriazole through the activation of PMS. This composite demonstrated a nearly 20 times higher rate constant than single $CoFe_2O_4$ nanoparticles. It is proposed that part of the reason for this is because both the cobalt ferrite and the-doped graphene oxides can contribute to the reaction as well as the composite having a greater surface area and a higher adsorption affinity for benzotriazole.

Reduced graphene oxide (rGO) was used as a support for magnetic iron oxide (Fe_3O_4) nanoparticles (average size, ~200 nm) enveloped in polypyrrole by Hu et al. [99] who used an in situ polymerization of a mixture of polyvinylpyrrolidone and pyrrole monomer around presynthesized Fe_3O_4/rGO. This composite material has a much lower magnetic response, but still can be mostly withdrawn from suspension in water using a magnet. These composites were tested for the adsorption of Pb^{2+} ions from water. It was demonstrated that this nanocomposite can adsorb Pb^{2+} with a maximum adsorption capacity of 93.2 $mg{\cdot}g^{-1}$ that is higher than is reported for Fe_3O_4/rGO (71.0 $mg{\cdot}g^{-1}$). The performance of this nanocomposite is more selective for Pb compared to other heavy metals such as Cd, Ni and Hg. Reusability studies have been conducted with desorption of the adsorbed Pb^{2+} with dilute nitric acid followed by repeated cycles of adsorption and it was reported that after five cycles to still show 85.7% adsorbance.

A small quantity of rGO was also combined with titanium dioxide (TiO_2) nanosheets (average size, 20 nm) and zinc ferrite ($ZnFe_2O_4$) by Kang et al. [100] who then tested this material for the photocatalytic degradation of p-nitrophenol. A composite with 3% *w*/*w* of rGO was demonstrated to degrade 99.7% of a 10 $mg{\cdot}L^{-1}$ p-nitrophenol solution under UV-vis light after 60 min. After 5 cycles of reuse the nanoparticles were reported to still degrading p-nitrophenol at 88.1% efficiency which indicates strong potential for use as a catalyst for the removal of contaminants from water. It is proposed that the rGO acts as a transfer medium allowing both the TiO_2 and $ZnFe_2O_4$ nanoparticles to contribute to ROS formation (Figure 4).

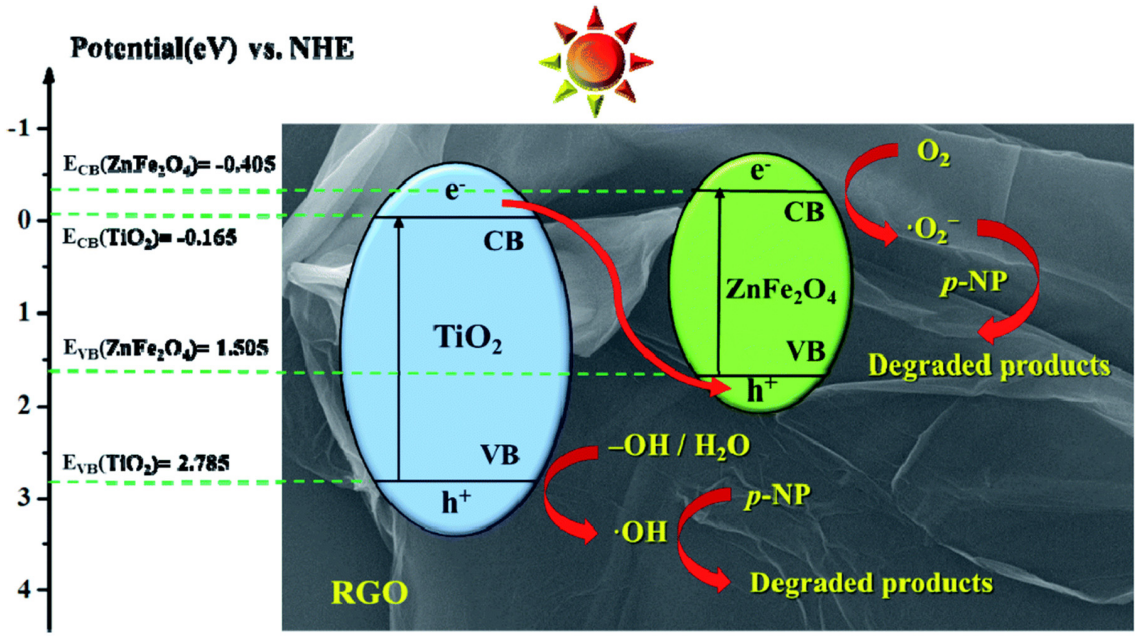

Figure 4. Possible mechanism for the formation of reactive oxygen species by $TiO_2/ZnFe_2O_4$/rGO nanocomposites. Images from Kang et al. [100]. Published By the Royal Society of Chemistry (RSC).

Sulfur and nitrogen co-doped graphene oxide was reported by Liang et al. [101] as a support for magnetite nanoparticles (average size, 33 nm) stabilized with *L*-cysteine through a hydrothermal synthesis. These three-dimensional composite structures demonstrated a magnetic response and were also investigated for the adsorption of the dye molecules methylene blue, Congo red and neutral red reporting maximum adsorption coefficients of 171.53, 909.09 and 877.19 $mg \cdot g^{-1}$, respectively.

Non-exfoliated graphite in conjunction with magnetite particles (average size, 100 nm) and polyethyleneimine synthesized through a solvothermal synthesis was reported by Qiu et al. [102] who demonstrated that this material showed promise as an adsorbent for humic acid with 49.87 $mg \cdot g^{-1}$ reported for the maximum adsorption coefficient.

Another carbon allotrope which can be modified with magnetic nanoparticles are carbon nanotubes (CNTs) as reported by Wang et al. [103] who decorated carbon nanotubes with bimetal ferrites (general formula $Co_{0.5}$ $M_{0.5}$ Fe_2O_4 where M can be Cu, Ni, Mn and Zn) (size range, 30–70 nm). They observed that all of these composites could adsorb pentachlorophenol (PCP) from water with values of 76.02, 75.80, 75.83 and 74.50 $mg \cdot g^{-1}$ for M equals to Cu, Mn, Ni and Zn, respectively. It was also observed that the PCP can be removed readily through the use of microwave irradiation (850 W, 100 s) which enabled the magnetic adsorbent to be reused at least six times with only a minor loss of efficacy (98.1% efficacy for M=Cu) and magnetic material (<7%).

Carbon nanotube-based composites were also examined for their effectiveness for the removal of cyanobacteria from water by Wang et al. [104] who synthesized Fe_3O_4 coated CNTs using an ultrasound synthesis and then tested the coagulation of *Microcystis aeruginosa* from water samples in the presence of the composites and aluminum sulfate ($Al_2(SO_4)_3$) under ultrasound. It was observed that the nanocomposite pre-oxidized the bacterial cells allowing up to 90% reduction in the bacterial load. It was also found that as the composites only served as a mild oxidant, they did not excessively damage the bacterial cells preventing the release of toxic cell breakdown products into the water.

Carbon nanotubes were also used by Liu et al. [105] who bound iron (average size, 5 nm), copper and copper oxide (average size of both, ~30 nm) nanoparticles to carbon nanotubes through a liquid phase reduction process. These composites when combined with nanotubes coated in aluminum nanoparticles (average size, 64 nm) can spontaneously oxidatively degrade the antibiotic sulfamerazine. It was reported that dissolved oxygen in the presence of the supported aluminum particles can generate H_2O_2 through a reduction process which is then converted to reactive oxygen species such as ·OH and $O_2^{\cdot -}$ (Figure 5). They reported that 85% of sulfamerazine and 60% of total organic content can be removed from water over the course of 60 min at pH 5.8 with constant O_2 flow.

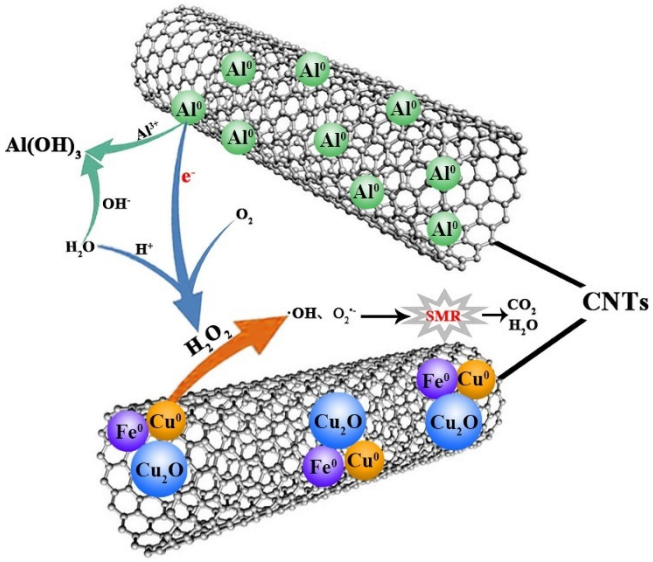

Figure 5. Reaction mechanism of the Al0-CNTs/CNTs-Fe–Cu system for the generation of ROS in the presence of O_2. Reprinted from Liu et al. [105] with permission from Elsevier.

Nanodiamond was also reported by Navalón et al. [106] who functionalized nanodiamond and other carbon containing supports through the use of Fenton reagent followed by chemical deposition of bimetallic nanoparticles through chemical reduction. It was observed that these composites can catalyze the Fenton reaction for the removal of phenol from water. A $Fe_{20}Cu_{80}$ cluster (average size, 5.4 nm) with a 0.2 wt% metal loading on nanodiamond was able to catalyze 90% reduction in a 100 mg·L^{-1} solution of phenol with a 1:6 ratio of phenol to H_2O_2 at pH 6. The catalyst proved reusable with no loss of function reported over three runs.

Less organized activated carbon was also reported by Lee et al. [107] as a surface for depositing nickel-doped iron (Ni_nFe) nanoparticles (size range, 20–70 nm) which were tested for the degradation of perfluorooctanesulfonate a common fire-retardant found leaching into the aquatic environment. Around 94% degradation of the contaminant was reported at 50 °C with fluorides and sulfites being common reaction products. The potential risks of these reaction products were not considered in this study. However, since perfluorooctanesulfonate has a legal safe limit of only 70 parts per trillion [109] while fluoride can be in drinking water up to 1.4 mg·L^{-1} [110] and the oxidized form of sulfite, sulfate can be tolerated at well over 1 g·L^{-1} over short timescales [111] this should be minor.

A series of different forms of carbon from carbon powder to graphene oxide to carbon nanotubes was used by Yang et al. [108] as supports for nZVIs (average size, <10 nm) that were then tested for the adsorption and reductive degradation of chloramphenicol, an antibiotic. Carbon black was the most effective support with close to 99% removal of a 0.30 mM chloramphenicol solution reported in 3 min. It is surmised that this carbon structure served best because it allowed the most even distribution of nanoparticles of any of the structures and a very high adsorption capacity (3000 mg·g^{-1}).

3.3. Polymer/Magnetic Nanomaterial Composites

Polymeric materials are another interesting potential material for the generation of nanocomposites (Table 6). They can act as bridges, linking many nanoparticles together into aggregate materials. Some polymers themselves can have chemical functionalities or other properties which participate in the function that the nanocomposite have been developed for. This type of nanocomposite was reported by Sun et al. [112] who investigated the adsorption efficiency of β-cyclodextrin polymer alone and when synthesized in the presence of Fe_3O_4 nanoparticles (size range, 20–30 nm) for the rare earth elements neodymium and gadolinium. While there was a small reduction of q_{max} for the polymer with magnetic nanoparticles for Nd and Gd from water (8.88 and 7.78 mg·g^{-1}) compared to the raw polymer (9.59 and 8.99 mg·g^{-1}) the presence of the magnetic nanoparticles not only improved the anticlogging performance and pressure resistance of the cyclodextrin, but also added the ability of the adsorbent to be collected with simple application of a magnet. Both forms of polymer were found to be highly selective for rare earth elements when in a mixture with other ions and could both be reused and recover useful elements with high efficiency through up to five cycles. Testing this composite with diluted wastewater from a rare-earth processing facility demonstrated selective adsorption of rare earth elements from a mixture of ions with significant rates of recovery ranging from a measured 107% for samarium and 62% for cerium.

Table 6. Magnetic nanocomposites made with polymers with reported targeted contaminant and method of removal.

Core MNP	Polymer of Additional Coating	Surface Area (m^2 g^{-1})	Contaminant	Method of Removal	Ref
Fe_3O_4	β-cyclodextrin	85	Nd, Gd, ions	Adsorption	[112]
Fe_3O_4	Poly-vinyl alcohol, sodium alginate	N/A	*Nannochloropsis oculata*	Flocculant	[113]
CuO and FeOOH	Ion exchange resin	18.9	As(V)	Adsorption + reduction	[114]

Table 6. *Cont.*

Core MNP	Polymer of Additional Coating	Surface Area (m^2 g^{-1})	Contaminant	Method of Removal	Ref
Fe_3O_4	Thiourea formaldehyde resin	132.6	CrO_4^{2-} and AsO_4^{3-}	Adsorption	[115]
Fe_3O_4	Molecular sieves carbon	522.7	Methyl orange, methylene blue rhodamine B dyes	Adsorption	[116]
Fe/Mn binary oxide	Polyvinylidene fluoride	N/A	As(V)	Adsorption	[117]
Fe_3O_4	α,α′-dichloro-p-xylene carbonized	180	U(VI)	Adsorption	[118]

The insertion of nanosized Fe_3O_4 nanoparticles (size range, 2.4–2.9 nm) into polyvinyl alcohol and sodium alginate beads was reported by Kao et al. [113] who used them as a flocculant for the removal of *Nannochloropsis oculate* algae from water. As the polymer sheath protects the magnetic core from degradation under acid conditions this provides an effective tool for the removal of algae from water.

An interesting form of composite was reported by Kociołek-Balawejder et al. [114] who formed a copper iron oxide (CuO and FeOOH) layer on the surface of ion exchange resin beads. These composites were reported to adsorb As(III) ions from water through their oxidation to As(V). Through this process the material adsorbs a maximum of 94.4 $mg{\cdot}g^{-1}$. When the resin beads were used and reused repeatedly it was demonstrated that the ability to adsorb As(III) and (V) is retained with a minimum of 88% removal over the course of nine cycles. The composite material was tested in a flow column system using model ground water spiked with As ions and it was observed that this system can reduce the As concentration from 500 $\mu g{\cdot}L^{-1}$ to less than 10 $\mu{\cdot}L^{-1}$ which is within the safe limit for human consumption. However, it was reported that this process took 23 days.

A magnetic thiourea–formaldehyde resin was utilized by Goonetilleke et al. [115] who formed such a resin in the presence of magnetite (Fe_3O_4) nanoparticles. These could extract chromium (IV) and arsenic (V) oxyanions (CrO_4^{2-} and AsO_4^{3-}) from water with maximum adsorption of 3.76 and 1.63 $mmol{\cdot}g^{-1}$ for Cr(IV) and As(V), respectively. Notably this capacity can be increased further through the use of ultrasound which can increase the adsorption of Cr(IV) and As(V) to 4.28 and 1.97 $mmol{\cdot}g^{-1}$, respectively. They also reported that the use of ultrasound can aid the desorption of the contaminants needing only 6–10 min compared to 80 min for the passive process and also needing less NaCl with 99.9% desorption with 0.3 M being sufficient using ultrasound while the passive process requires 1.5 M. This demonstrates another interesting method for the use and reuse of adsorbent materials for water remediation.

Molecular sieves were used as the template for the formation of grape-like clusters (average size, 360 nm) of carbon to which Fe_3O_4 nanoparticles had been coated through a solvothermal synthesis by Tian et al. [116] They investigated the adsorption capacity for methyl orange, methylene blue and rhodamine B dyes with reported values of 400, 600 and 150 $mg{\cdot}g^{-1}$, respectively.

Polymer/magnetic binary oxide nanofibers were reported by Akhgar et al. [117] who generated the nanofibers by electrospinning a mixture of polyvinylidene fluoride and Fe–Mn binary oxide nanoparticles (average size, <4 nm). The resulting fibers were tested for adsorbance of arsenic from water and found to exhibit a maximum adsorbance capacity of 21.32 $mg{\cdot}g^{-1}$ at pH 7. It was also found that the adsorbent could be regenerated using a basic bleach solution and still retain up to 70% of its adsorption capacity.

A magnetic tubular nanocomposite was reported by Zhang et al. [118] who generated carbon fibers (average diameter, 100 nm) through the carbonization of self-polymerized α,α′-dichloro-p-xylene which were then coated with either carboxylic acid (-COOH) or sulfonic acid ($-SO_3H$) groups followed by the growth of Fe_3O_4 nanoparticles onto the tubes through a basic reflux (Figure 6). These tubular structures were found to adsorb uranium (VI) at high effectiveness with over 99% of a 5 $mg{\cdot}L^{-1}$

solution removed at pH 8 for the sulfonic acid functionalized composites. When the maximum adsorption coefficient (q_m) was determined for these nanotube structures it was determined to be 980.4 and 955.7 mg·g^{-1} for the -SO_3H and -COOH functionalized tubes, respectively. When tested against simulated seawater the composites demonstrated a high degree of removal (at least 80%) of the U(IV) present though there was some competition for adsorption sites with VO_3^- ions. When tested for reusability these nanocomposites still demonstrated close to 90% adsorption on the sixth cycle of use/reuse.

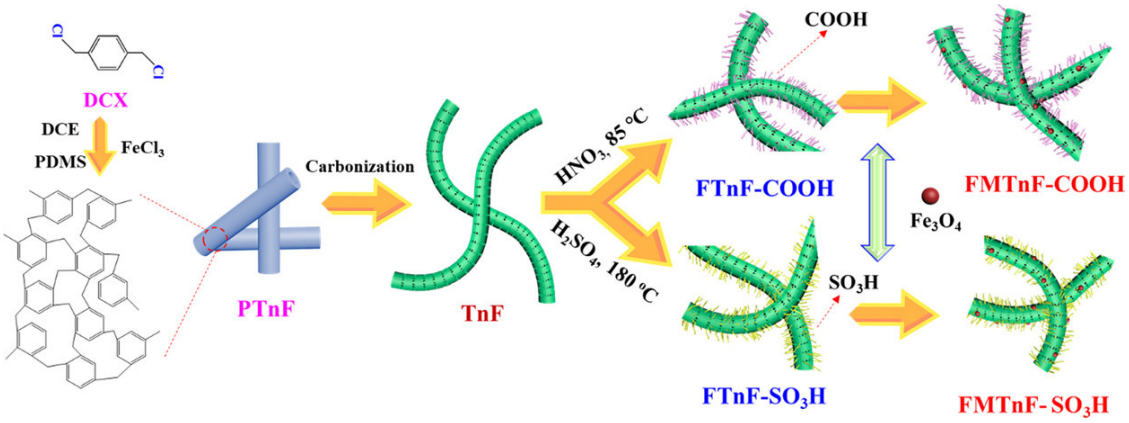

Figure 6. Systematic reaction pathway for the generation of COOH or SO_3H coated magnetic nanowires. Reprinted with permission from Zhang et al. [118] Copyright 2020 American Chemical Society.

3.4. Metallic/Metal Oxide/Magnetic Nanoparticle-Based Nanocomposites

The inclusion of metals, metal oxides and other inorganic materials into nanocomposites has also been reported many times in recent literature (Table 7). Metal and metal oxide nanomaterials have chemical and physical properties that make them suitable for the removal of contaminants from water. The addition of magnetic nanoparticles aids this application as recovery and reuse can be facilitated.

Table 7. Examples of magnetic nanocomposites formed with inorganic materials such as metals, metal oxides and metal organic frameworks.

Core MNP	Metal oxide Component	Surface Area (m^2 g^{-1})	Contaminant	Method of Removal	Ref
$CoFe_2O_4$	Ag_2O	N/A	Methyl orange	Photocatalysis	[119]
Co_2O_3	Cu_2O_3:Al_2O_2	N/A	Various bacteria	Bacterial inhibition	[120]
$MnFe_2O_4$	ZrO_2	N/A	Methylene blue	Decolorization	[121]
Fe_3O_4	SiO_2	275	Pb^{2+}	Adsorption	[122]
nZVIs	SiO_2	N/A	Organic arsenic compounds	Fenton reaction + adsorption of waste product	[123]
nZVIs	Pd	10.9	Carbon tetrachloride	Reduction	[124]
Fe_3O_4	SiO_2	N/A	Aniline	Adsorption	[125]
$FeNi_3$	SiO_2+TiO_2	N/A	Humic acid	Photocatalysis	[126]
$FeNi_3$	SiO_2+ZnO	N/A	Tetracycline tamoxifen	Photocatalysis	[127,128]
$FeNi_3$	SiO_2	481.6	Tetracycline metronidazole	Fenton catalysis	[128,129]
Fe_3O_4	TiO_2	29.4	Rhodamine B	Photocatalysis	[130]
Iron oxide (industrial waste)	TiO_2	N/A	Organic dyes and bacteria	Photocatalysis	[131]

Table 7. *Cont.*

Core MNP	Metal oxide Component	Surface Area (m^2 g^{-1})	Contaminant	Method of Removal	Ref
$ZnFe_2O_4$	V_2O_5 (e-waste)	N/A	BTEX	Fenton catalysis	[132]
γ-Fe_2O_3	Mn–Fe Oxide	109	As(v) + as(iii)	Adsorption	[133]
$CoFe_2O_4$	ZnO_2	N/A	Acid blue 113	Radical generation	[134]
$CuFe_2O_4$	CuO	N/A	Methylene blue	Photocatalysis	[135]
FeOOH	Al_2O_3	267	Humic acid	PMS activation	[136]
$Co_{0.5}Ni_{0.5}FeCrO_4$	UiO-66 MOF SWCNT-GO	210.5	4-nitrophenol 4-aminophenol	Reduction	[137]
nZVIs	ZIF-67 MOF PVP	254.5	Cr(VI)	Adsorption + reduction	[138]
Fe_3O_4	Ag	N/A	Rhodamine B methylene blue nitrophenol	Reduction	[139]
Fe_3O_4	SiO_2	568	Pb^{2+} + methyl orange	Adsorption	[140]

The formation of hollow porous Fe_3O_4 microspheres (average size, 200 nm) to which silver nanoparticles were grafted was reported by Zhang et al. [141] who used a hydrothermal method after the reduction of silver nitrate by sodium borohydride or tri sodium citrate. These nanocomposites were examined for the catalytic reduction of p-nitroaniline and were found to promote near complete reduction in less than 10 min in an excess of borohydride with a first-order rate constant of 0.45 min^{-1}, a value that compares well to the literature.

Jiang et al. [119] reported the development of a through put system for the degradation of organic dyes in water. The system that they developed, called a magnetic aggregation bed photocatalytic reactor, contained a photocatalytic reactor cell with a line of attached permanent magnets. When a magnetically active photocatalyst is added to the through-stream—in this case cobalt ferrite with silver oxide ($CoFe_2O_4$–Ag_2O) (average size 30–50 nm)—they aggregate at the points in the reactor with the highest levels of magnetic field (Figure 7). By adjusting the position and strength of the magnets the structure of the aggregates can be changed from flowers to branches. Passing a simulated wastewater stream with methyl orange through the reactor using natural light they were able to achieve close to 95% degradation of a 16 mg·L^{-1} after 60 min.

Figure 7. Photograph showing $CoFe_2O_4$@Ag_2O nanocomposites arranged in a photochemical reaction with different strengths of magnetic field. Reprinted from Jiang et al. [119] with permission from Elsevier.

An interesting level of control of the synthesis regime can lead to varying degrees of control of the magnetic and antimicrobial nanocomposites. This was demonstrated by King Abia et al. [120] who grew cobalt oxide (Co_2O_3) nanoparticles (average size 22–33 nm) on a copper aluminum silica Cu_2O_3:Al_2O_2 matrix through the use of a sol–gel method. The magnetic response was reported to be dependent on the concentration of cobalt added to the reaction mixture. These nanocomposites were tested for their antibacterial activity under both laboratory settings and using samples of river water. They showed almost complete inhibition of such bacterial species as *E. coli*, *S. enterica*, *S. aureus* and *L. monocytogenes* in some cases as quickly as only after 20 min of exposure. They reported that the presence of cobalt nanoparticles increases the antibacterial activity of the nanocomposites. The nanocomposites were also determined to be nontoxic to human epithelial-line 2 cells indicating that they may be suitable to use in preparing water for human consumption.

Zirconium oxide (ZrO_2) nanoparticles have been attached to manganese ferrite ($MnFe_2O_4$) nanoparticles (average size, <20 nm) by Nagabhushana et al. [121] who investigated this material as a potential material for the decolorization of organic dyes in water. It was found that at pH 7 the nanocomposite was able to degrade up to 95% of a 20 ppm methylene blue dye solution within 90 min under natural light. This nanocomposite was also tested against wastewater from textile production containing a series of dyes and it was found that only 59% of discoloration was reported. It is indicated that this reduction in the rate of degradation is due to the number of other species which would compete for active sites on the composite reducing the overall level of degradation.

Another form of oxide nanomaterial formed in the presence of magnetic nanomaterials was reported by Putz et al. [122] who formed iron oxide nanomaterials (average size, 10 nm) and then coated them in a layer of nanoscale silicon dioxide using the Stöber method. These magnetic composites were then tested for the removal of Pb^{2+} from water and achieved adsorption efficiencies of 14.9 $mg{\cdot}g^{-1}$ through what is suggested as a primarily surface-based process and which achieved over 95% Pb^{2+} recovery after washing with mild acid making possible its reuse.

In an interesting report, Liu et al. [123] coated nZVIs (average size, 20–40 nm) with SiO_2 which were then investigated for the removal of organoarsenic compounds from water. It was reported that the nanoparticles served to act not only as a catalyst for the heterogenous Fenton treatment for degradation of the organic component, but also that the FeO and FeOOH groups on the surface of the nanoparticles served to adsorb the inorganic arsenic that was generated in the degradation reaction. As such, these nanoparticles also reduced the toxicity of water that had contained the contaminants. Interestingly, the presence of the SiO_2 layer greatly increased the rate of degradation of contaminant compared to uncoated iron particles.

Zerovalent iron was also reported by Bhattacharyya et al. [124] who palladized or sulfurized these particles (average size, 70 nm) and then investigated these particles for the degradation of carbon tetrachloride in deoxygenated water. The palladized nanoparticles demonstrated high activity and were demonstrated to degrade carbon tetrachloride with over 99.9% removal of a 25 mM solution. The degradation process can continue multiple times while retaining activity. It was also reported that the catalyst can then be regenerated using borohydride.

Silicon dioxide coated iron oxide was also reported by Labuto et al. [125] who formed both the core Fe_3O_4 nanoparticles and SiO_2 shell through electrochemical processes which did not require surfactants or other stabilization agents. The resulting nanocomposites were tested for the adsorption of aniline from water and demonstrated a high maximum adsorption capacity of around 126.6 $mg{\cdot}g^{-1}$ at pH 6 and 50 °C. Silicon dioxide was also reported by Mazarío et al. [140] who generated Fe_3O_4/SiO_2 core shell nanoparticles (average size, 50.3 nm) in the presence of the porogenic agents hexadecyltrimethoxysilane or octadecyltrimethoxysilane which then generated mesoporous SiO_2 outer layers for the nanocomposites. After calcination at 400 °C, these composites demonstrated good adsorption of Pb^{2+} ions and methyl orange.

Magnetic iron nickel ($FeNi_3$) particles with an inner shell of silicon dioxide (SiO_2) and an outer shell of titanium dioxide (TiO_2) with a diameter of 10 nm for the core and 12 and 70 nm after the edition of SiO_2 and TiO_2 respectively was reported by Panahi et al. [126] who tested this composite for the photocatalytic degradation of humic acid from water under UV irradiation. Close to 100% degradation was reported. Similar composites with zinc oxide (ZnO) in the outermost shell as opposed to titanium dioxide (average size, 39 nm) was reported both by Khodadoost et al. [127] and Panahi et al. [128] who both demonstrated the ability to photocatalytically degrade organic contaminants, namely the antibiotic tetracycline and the anticancer drug tamoxifen both with 100% efficiency under simulated sunlight. $FeNi_3$@SiO_2 composites, (size range, 45–50 nm), which do not possess a third outer shell were reported by Mahvi et al. [128] and Allahresani et al. [129] who used the composites for the Fenton style catalytic degradation of tetracycline (87% removal) and metronidazole (84% removal), respectively.

Magnetic photocatalytically active 1D composites structures have been reported by Wang et al. [130] who synthesized titanium dioxide (TiO_2) nanotubes through electrochemical etching followed by insertion of oleic stabilized magnetite (Fe_3O_4) nanoparticles (average size, <10 nm) which were converted to Fe_2O_3 and incorporated into the structure. These nanocomposites demonstrated a strong magnetic response and were photocatalytically active under visible light. They were able to degrade over 86% of a rhodamine B dye solution. The catalyst was easily recovered using a magnet and was reused up to three times with minor loss of activity.

A very interesting method for the formation of titanium dioxide coated magnetic nanocomposite was reported by Das et al. [131] who treated iron oxide containing industrial waste with ball milling forming particles with a size range between 5 and 2 nm. These composites demonstrated very good photocatalytic activity for degradation of rhodamine B, Congo red and methylene blue as well as *E. coli* bacteria. This material showed a strong case of reusability with the reported level of methylene blue degradation remaining high over 10 cycles.

A similar structure was reported by Oh et al. [132] who generated vanadium oxide (V_2O_5) nanoparticles (average size, 50 nm) and joined them to zinc ferrite nanoparticles ($ZnFe_2O_4$) nanoparticles through a solvothermal process. These composite materials were found to be photocatalytic again benzene, toluene, ethylbenzene and xylene (BTEX) contamination in water. At pH 3 the composite was able to achieve close to 95% degradation of a BTEX solution in 90 min. This value could be raised to 98% through the addition of H_2O_2 to the reaction medium. Most notably about this work, the vanadium nitrate used for the synthesis was sourced from electronic waste. This indicates a potential for a circular economy whereby waste materials are used for the remediation of contamination from industrial activity.

A manganese iron binary oxide was grafted onto the surface of iron oxide nanoparticles (average size, 21 nm) by Agbaba et al. [133] who then tested this material for the removal of arsenic species from water. These composite materials were found to have maximum adsorbance capacities of 55.9 $mg{\cdot}g^{-1}$ for As(III) and 54.1 $mg{\cdot}g^{-1}$ for As(V) at pH 7. In the case of As(III) the reported values is more than twice as large as that reported for unfunctionalized magnetic nanoparticles (25.5 $mg{\cdot}g^{-1}$) while it is only slightly higher than the value reported for As(V) (50.9 $mg{\cdot}g^{-1}$). It was determined that the adsorption of As(III) species occurred through an oxidation pathway involving Mn species in the binary oxide accounting for the large increase in As(III) adsorption. It was also observed that oxidation of the surface of the composite using a mild bleach allowed the composite to be reused over at least five cycles.

Cobalt ferrite ($CoFe_2O_4$) nanoparticles were synthesized in the presence of zinc oxide (ZnO_2) nanoparticles (average size, 30–40 nm) by Anandan et al. [134] who used a novel low frequency ultrasound-based synthesis. These novel composites were tested for the catalytic degradation of Acid Blue 113 dye in water. The nanocomposite showed much higher rates of degradation compared to the individual component nanoparticles and could reduce the total organic component of a water sample in a shorter period of time. These nanocomposites were also examined for reuse and still demonstrated 90% activity after 6 cycles of drying and reuse.

Copper ferrite ($CuFe_2O_4$) with copper oxide (CuO) was reported by Rabbani et al. [135] who synthesized the ferrite (size range, 170–195 nm) using a mixture of ultrasonication and solvothermal synthesis followed by decoration with CuO using ultrasonication followed by calcination. The resulting composite demonstrated a strong magnetic response and was able to degrade up to 90% of a 10 $mg{\cdot}L^{-1}$ solution of methylene blue.

Alumina (Al_2O_3), was bound to iron oxide (FeOOH) nanoparticles by Wang et al. [136] through a hydrothermal hydrolysis process. This composite was then tested for use as an activation catalyst for PMS. The composite was tested for the removal of humic acid from water and up to 93% of a 30 $mg{\cdot}L^{-1}$ solution of humic acid was degraded at pH 7 and the same performance can be repeated at least four times. The presence of phosphate ions was reported to reduce considerably the activity of the catalyst while chloride ions did not have a noticeable effect.

Metal organic frameworks (MOFs) in conjunction with single walled carbon nanotubes (SWCNT) and graphene oxide (GO) sheets were joined with magnetic nanoparticles in order to form composite materials by Freiss et al. [137] In this work, $Co_{0.5}Ni_{0.5}FeCrO_4$ particles (average size 41.5 nm) were synthesized through a sol gel method and then surrounded by UiO-66 MOF to which was then bound SWCNTS or GO. After full characterization, these materials were tested for potential application in water remediation by catalyzing the reduction of 4-nitrophenol to 4-aminophenol.

A MOF was also reported by Hu et al. [138] who enveloped PVP stabilized nZVIs with ZIF-67 MOF that was then carbonized to form nZVI@ZD composite (average diameter, 0.7 μm). This nanocomposite was tested for the removal of Cr(VI) ions from water and was reported to have a maximum adsorption capacity of 226.5 $mg{\cdot}g^{-1}$, far higher than what was observed for the free zerovalent iron and the composite before carbonization. It was determined through XPS analysis that the Cr(VI) ions enter the composite through pores in the structure and are converted into Cr(III) ions through reduction which were then adsorbed and retained by precipitation inside the porous structure.

Silver nanoparticles were also bound to Fe_3O_4 nanoparticles (average size, 20 nm) as reported by Patil et al. [139] who then tested these composites in the reduction of 50 ppm solutions of organic dyes. It was observed that these nanocomposites achieved over 98% reduction of rhodamine B, over 80% of methylene blue and over 97% of nitrophenol in the presence of sodium borohydride in less than 5 min. After recovery by magnet the catalytic activity of this nanocomposite was not determined to have been reduced significantly.

3.5. Conclusions

In conclusion, four different groupings of magnetic nanocomposite material have been presented. With clay-based magnetic nanocomposites, various natural and artificial clays were prepared and joined with magnetic nanomaterials. These composites demonstrated good adsorption behavior, and some could catalyze the oxidative removal of contaminant species. With carbon-based nanomaterial composites excellent adsorption activity was observed and interesting behavior where the carbon material served as a support which aided other bound nanomaterials in performing reactions. Polymer magnetic nanocomposites demonstrated contaminant removal primarily through adsorption. It should be noted that the presence of iron-based nanoparticles could improve the adsorption behavior of polymers as there can be reactions that reduce contaminant species and trap them in the composites. Metal and oxide magnetic nanocomposites could be generated that demonstrated both catalytic and adsorption behavior. Interestingly, in several cases, the metal oxide used can be sourced from waste material which would be of interest to those seeking to reduce the environmental impact of the remediation activity.

4. Magnetic Biological Nanocomposites

The development of nanocomposites containing biological materials has already been reported in a series of reviews in recent years [30,142,143]. There does, however, continue to be rapid development in the field.

4.1. Biologic Polymer/Magnetic Nanocomposites

One of the more interesting forms of biological material which may be used for the generation of nanomaterials would be the use of biopolymers (Table 8). These readily available and chemically interesting materials may prove an interesting and effective component of composites for the removal of contaminants from water resources.

Table 8. Magnetic nanocomposites with biological polymers and extracts.

Core MNP	Biopolymer	Surface Area (m^2 g^{-1})	Contaminant	Method of Removal	Ref.
Fe_3O_4	Humic acid	68	Malachite green	Adsorption + degradation	[144]
Fe_3O_4	Humic acid	N/A	Carbamazepine, ibuprofen, bisphenol A, 5-tolylbenzotriazole	Fenton photocatalysis	[145]
Fe_3O_4	Lignosulfonate	53.8	Congo red, titan yellow	Adsorption	[146]
Fe–Mn binary oxide	Starch	N/A	As(III) and Cd(II)	Adsorption	[147]
Fe_3O_4	Bean extract	78.6	Indigo carmine	Adsorption	[148]
Iron oxides	Chitosan	N/A	Sr90	Adsorption	[149]
Fe_3O_4	Chitosan	N/A	Microcystin LR	Adsorption	[150]
iron	Chitosan	N/A	As(V)	Adsorption	[151]
Fe_3O_4	Chitosan/polyaniline	N/A	CrO_4^{2-}	Adsorption	[152]
Fe_3O_4	Chitosan	N/A	Sunset yellow dye	Adsorption	[153]
Fe_3O_4	chitosan + SnO_2	3.6	Reactive brilliant red	Adsorption	[154]
α-Fe_2O_3	Cellulose acetate	N/A	Bacteria	Inhibition	[155]
nZVIs	Microcrystalline cellulose	23.4	Pb^{2+}	Adsorption	[156]
$CoFe_2O_4$	Pectin (from orange juice production)	N/A	Oil emulsion	Adsorption	[157]
CuO/Fe_2O_3	Loquat extract	13.4	Norfloxacin, ciprofloxacin	Adsorption	[158]
$ZnFe_2O_4$	Black pepper extract	N/A	Methylene blue	Photocatalysis	[159]
$Ni_{0.1}CuO$	Gum acacia	N/A	Various bacteria	Inhibition	[160]
Iron oxides	Myrrh gum	N/A	Crude oil	Adsorption	[161]
Fe_3O_4	Onion peels, corn-silk husks	243 261	As species	Adsorption	[162]
Magnetic iron oxide	Bovine serum albumin	70.6	PO_4^{3-}	Adsorption	[163]
nZVI	Extracellular polymeric substances (EPS)	N/A	SB(V)	Reduction	[164]
S–nZVI	EPS from sewage sludge	N/A	Nitrobenzene	Reduction	[165]

A recent study by Tiwari et al. [144] demonstrates the synthesis of Fe_3O_4 nanoparticles stabilized with humic acid. These magnetic particles (average size, 14 nm) can adsorb malachite green dye of with a Langmuir isotherm adsorption close to 160 $mg{\cdot}g^{-1}$ at 50 °C. These materials can then catalyze the breakdown of the dye when subjected to ultrasonication as the thermal energy of the sonication is converted into OH radicals which can then degrade the dye molecules. It was observed that through these two mechanisms a concentration of dye of up to 200 $mg{\cdot}L^{-1}$ can be 100% degraded in as little as 40 min. Prevot et al. [145] reports a similar co-precipitation, but then reports the use of this material as a photocatalyst for the Fenton reaction in the presence of sunlight. Using this material and hydrogen peroxide (H_2O_2) the particles were observed to degrade various contaminants of emerging concern (CECs) such as carbamazepine, ibuprofen, bisphenol A and 5-tolylbenzotriazole both in deionized

water and in simulated wastewater. Different syntheses for the particles were reported with variations in the weight percentage of humic acid used. It was reported that 0.5 wt% showed the highest performance with complete degradation in less than 5 min.

Another biological material which has been reported as a feedstock for materials for the remediation of water was lignin. In a report by Wang et al. [146] a lignin-based surfactant lignosulfonate was used as a stabilizer for the synthesis of Fe_3O_4 nanoparticles (size range, 100 and 200 nm). These were shown to have good adsorption for Congo red and titan yellow dyes demonstrating maximum adsorbance capacities of 198.24 and 192.51 $mg{\cdot}g^{-1}$, respectively. A high degree of reusability was reported in both cases with over 80% adsorbance remaining after five cycles. In a report by Liu et al. [166], it was observed that lignin sourced activated carbon can be made magnetic through alkaline hydrolysis followed by thermal treatment under nitrogen with the addition of $Fe(NO_3)_2$ and $Zn(NO_3)_2$. The resulting composite contained $ZnFe_2O_4$ nanoparticles (size range, 30–50 nm) and showed a high degree of adsorption of p-arsanilic acid (201.64 $mg{\cdot}g^{-1}$) at lower pH (<pH 4.0). This value was higher than the adsorbance value reported for activated carbon generated from lignin without the magnetic component. It was observed that this high degree of adsorption may be identified with a mixture of interactions between the nanocomposite and the p-arsanilic acid molecules such as electrostatic attraction, surface complexation, π-π stacking and hydrogen bonding interactions. The authors report that this lignin-based magnetic activated carbon can be synthesized through a very straight-forward, cheap synthesis so would be an excellent choice for the removal of organic arsenic from water sources.

Starch is another material of biologic origin which has been incorporated into magnetic nanocomposites. In work reported by Tang et al. [147] calcium modified, starch stabilized ferromanganese binary oxides were generated. The synthesis of the binary oxides involved the dissolution of salts of iron and manganese with a starch solution followed by the addition of potassium permanganate (K_2MnO_4) with stirring for 24 h. After washing, filtration and drying the resulting composite was dispersed in water with different weight percentages of calcium carbonate ($CaCO_3$). It was proposed that the carbonate salt reduces the number of acidic surface groups in the composite and, as a result, enhances the adsorption properties of the nanocomposite surface. The composite showed a wide size distribution from a few tens of nanometers to 500 nm and was tested for the adsorption of As(III) and Cd(II) ions in water solution at pH 6 and achieved a maximum adsorbance of 156.25 $mg{\cdot}g^{-1}$ for As and 107.53 $mg{\cdot}g^{-1}$ for Cd, both very high values compared to similar materials in the literature. The authors propose that the pH of around 6 shows the best performance as at higher pH the Cd(II) ions begin to precipitate as hydroxide and negative charges repel As(III) ions while at lower pH a proton layer is formed on the composite surface reducing the number of effective binding sites. It was reported that spectroscopic analysis indicated that Fe species on the surface form a ternary complex with As and Cd which aids in the retention of these species on the nanocomposite surface.

Starch was also used by Oladebeye [167] who used the starch extracted from Jack Beans in order to create Fe_3O_4 nanoparticles (average size 1 nm). As of yet, these composites have not been tested for the removal of contaminants however their increased swelling compared to free starch particles indicates a high potential as an adsorbent.

The extract of a bean as stabilization agent was also reported by Kolekar et al. [148] who reported that Bengal gram bean can be used to form an extract that can then be used for the synthesis of Fe_3O_4 nanoparticles. These where then tested for the adsorption of indigo carmine dye and demonstrated a adsorption capacity q_m of around 394 $mg{\cdot}g^{-1}$. It was observed that close to 100% of dye can be removed and that this dye can be removed by shaking in deionized water followed by filtration. It was reported that over five cycles of this process the nanocomposite still maintained over 96% removal.

The biopolymer chitosan was tested as a stabilization agent for the generation of novel magnetic nanocomposites in comparison with KU 2–8 resin by Zemskova et al. [149]. While both materials demonstrated a high degree of adsorption of Strontium 90 (Sr^{90}) there was a higher degree of adsorption by the chitosan under basic conditions (0.1 M NaOH solution) while the resin exhibited better performance in the presence of salt solution (0.1 M NaCl solution).

Chitosan as a stabilizing agent for Fe_3O_4 nanoparticles (average size, ~20 nm) was also reported by Pan et al. [150] who tested these nanocomposites for the removal of microcystin LR, an environmental toxin generated by excess cyanobacteria growth in water. The maximum adsorption capacity for this composite was reported to be 589 $\mu g \cdot g^{-1}$ at a pH of 5.53 and at 40 °C. Reusability studies indicate a retention of adsorption activity through five cycles.

Chitosan was also reported in composites with magnetic nanoparticles and silver nanoparticles by Hadimani et al. [168] which were then incorporated into PVP polymer wires. These wires still showed limited magnetic behavior and their potential use as electromagnetic blockers has been suggested. They have also been examined for potential antibacterial activity and some versions of the wires showed activity against pathogen bacteria especially *E. faecalis* and *E. coli*.

Chitosan microspheres impregnated with iron were reported by Zaritzky et al. [151] to be generated through an ionotropic gelation in the presence of iron nitrate. These microspheres were examined for the adsorption of As(V) from water with close to 98% of a 0.3 $mg \cdot L^{-1}$ solution adsorbed over 24 h. The maximum adsorption capacity for this material was reported to be 120.77 $mg \cdot g^{-1}$ with negligible reduction in adsorption activity over 4 cycles of use and reuse and limited effect of the presence of other anions such as phosphate and carbonate in the solution.

Chitosan in conjunction with polyaniline was used by Huang et al. [152] who synthesized magnetite (Fe_3O_4) (average size, 25 nm) in a chitosan matrix and then coated these composites with polyaniline through the use of a polymerization reaction of aniline. This nanocomposite was tested for the removal of chromium (VI) (CrO_4^{2-}) from water and reported a maximum adsorbance capacity of 186.6 $mg \cdot g^{-1}$ in acid pH. Adsorption analysis indicated that the process could occur both through direct adsorption of the chromium ions and reduction of the chromium by the polyaniline allowing chelation of Cr(III) ions. After elution by 1 M NaOH solution the composite could be reused with only 90% reduction in capacity after four cycles. chitosan in conjunction with polydopamine and the carbon-coated magnetic component of fly ash was formed into beads up to 60 µm in diameter by Li et al. [169] who then tested this material for use as an adsorbent for Ag^+ ions in solution. They reported a maximum adsorption capacity of up to 23.76 $mg \cdot g^{-1}$ and the presence of other metal ions does not greatly affect the adsorption capacity of the beads due to the distinctive coordination mechanism of Ag^+ compared to the other metals tested. It was also reported that the material is easily reused after treatment with an acidic sodium thiosulfate solution with more than 95% activity seen after 5 cycles.

In a similar work. chitosan mixed with prefabricated 50 nm-diameter Fe_3O_4 nanoparticles (average size, 50 nm) was crosslinked and polymerized with poly(acryloyloxyethyltrimethyl ammonium chloride) (PDAC) in order to form magnetic beads with a size range between 100 and 200 µm by Sarfaraz et al. [153] (Figure 8) who then tested them for the removal of inorganic chromium (VI) ions and organic sunset yellow dye. The composites showed maximum adsorption capacities for chromium (VI) ions and sunset yellow dyes of 163.93 $mg \cdot g^{-1}$ and 769.23 $mg \cdot g^{-1}$, respectively with moderately better performance at lower pH and a high degree of reusability for the removal of both contaminants.

Crosslinking chitosan was also reported by Cui et al. [154] who mixed iron oxide (Fe_3O_4) (average size, 20 nm) and tin oxide (SnO_2,) (average size, 50–70 nm) nanoparticles in crosslinked chitosan. The presence of the two nanoparticles enabled the maximum adsorbance capacity of reactive brilliant red of the composite to be raised close to unity (981.23 $mg \cdot g^{-1}$). The reusability of this composite was examined and it was demonstrated to have over 80% functionality after 5 cycles.

Another reported biological polymer utilized in magnetic composites was reported by Silva et al. [155] who blended α-hematite (Fe_2O_3) nanoparticles, (size range, 50–100 nm), with cellulose acetate polymer and formed nanocomposite films. These films were tested for antimicrobial activity against the Gram-positive bacteria *S. aureus* and the Gram-negative *E. coli* and *P. aeruginosa* and demonstrated biocidal activity with up to 78% of *P. aeruginosa* inhibited in the test medium after 24 h of exposure. It is suggested in the report that nanoparticle size aids their antimicrobial activity as the films with smaller nanoparticles showed higher biocidal activity. Ye et al. [156] also used cellulose-based

polymers synthesized through the acid hydrolysis of microcrystalline cellulose onto which nZVIs (size range, 50–100 nm) were deposited through the reduction of iron sulfate. This composite was examined for the adsorption of Pb^{2+} from water and was found to exhibit an impressive maximum adsorption capacity of 653.59 $mg{\cdot}g^{-1}$ with over 70% of the adsorption capacity being retained after 5 cycles of reactivation through dissolution with acid followed by reduction.

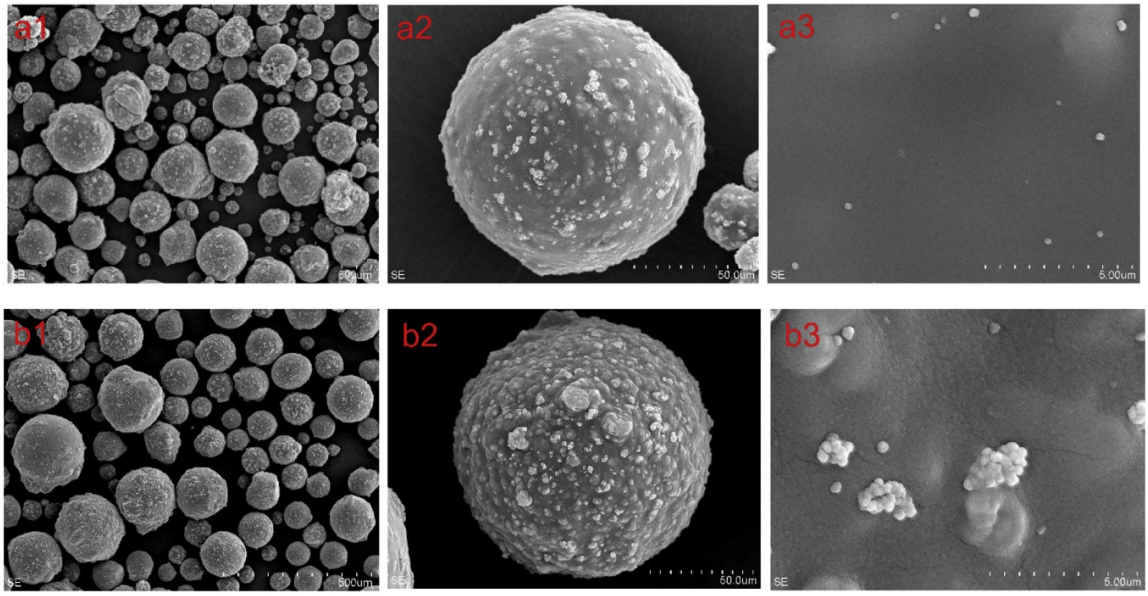

Figure 8. SEM images of (**a1**–**a3**) Fe_3O_4-chitosan spheres and (**b1**–**b3**) Fe_3O_4-chitosan PDAC spheres. Reprinted from Sarafaz et al. [153] with permission of Elsevier.

Another interesting report by Passamani et al. [157] demonstrated the use of residues from orange juice production as stabilizers in the production of magnetic cobalt ferrite ($CoFe_2O_4$) nanoparticles (size range, 80–140 nm). The authors utilized pectin polymer extracted from two different sources, the albedo of an orange and the residue from juice production and the dried residue from juice production without any further processing. The three stabilizer sources all lead to the production of high quality $CoFe_2O_4$ nanoparticles. These were all tested for the removal of oil from water and it was reported that the nanoparticles synthesized from pectin extracted from the residues of juice production demonstrated the very high level of extraction of 8 g of oil per gram of composite.

Another biological extract that was used for the generation of magnetic nanoparticles was reported by Zou et al. [158] who utilized an extract from the leaves of loquat, a popular fruit tree, for the synthesis of copper iron oxide nanoparticles (CuO/Fe_2O_3) (size range, 100–200 nm). These nanocomposites were demonstrated to adsorb the antibiotics norfloxacin (NOR) and ciprofloxacin (CIP) from aqueous solution. Interestingly, pH has a strong effect of the adsorption activity of CuO/Fe_2O_3 with a five-fold increase in adsorption capacity of NOR as pH was raised from 2 to 7 and a four-fold increase for CIP as the pH is raised from 2 to 8. This increase in adsorbance with a rise in pH did not continue, however. The adsorption efficiency of NOR was reduced by over 30% as pH values were raised from 7 to 11 and CIP demonstrated a decrease of over 10% as pH was raised from 8 to 11. The authors proposed that this is due to electrostatic effects as changes in pH causes protonation and deprotonation of the carboxylic and piperazinyl groups of the antibiotics as well as the surface of the adsorbent. Ali et al. [159] reports the use of an extract from black pepper *Piper nigrum* for the synthesis of zinc ferrite ($ZnFe_2O_4$) nanoparticles (size range, 60–80 nm) which were then demonstrated as photocatalysts for the degradation of the organic dye methylene blue. Close to 100% of a 15 ppm solution of methylene blue was degraded in 90 min at pH 7 with irradiation with sunlight.

Gum acacia, a complex polysaccharide extracted from certain trees of the genus *Acacia* was reported as a stabilizing agent in the generation of nickel-doped copper oxide nanoparticles ($Ni_{0.1}CuO$) (size average, 12 nm) by Singh et al. [160] who then examined the antibacterial activity of these nanocomposites against various pathogenic bacteria, namely *Enterobacter*, *Klebsiella pneumoniae*, *P. aeruginosa* and *S. aureus*. It was reported that this nanocomposite generated wider zones of inhibition than the commonly used antibiotic ampicillin and the same nanoparticles without gum acacia coating both with and without nickel doping.

Myrrh gum extract was also reported as a stabilization agent for the formation of magnetic nanoparticles (size average, 8 nm) by Diab et al. [161] who used these nanoparticles for the extraction of crude oil from water. Up to 95% of crude oil was removed using a 1 to 1 mass ratio of oil to MNPs. The report also details the phytoremediation quality of water hyacinth plants which enables supposed that a mixture of first treatment with magnetic nanoparticles followed by the use of appropriate plants may serve as very effective treatment of water contaminated by crude oil.

In a report by Agbaba et al. [162] extracts from onion peels and corn-silk husks were used for the synthesis of magnetite nanoparticles (size range, 26–28 nm) through a green synthesis. They were then tested for the adsorption of arsenic species in water. It was found that the nanoparticles made with onion peels and corn silk sourced nanoparticles both demonstrate higher levels of adsorption compared to nanoparticles generated using conventional chemical synthesis with 1.86, 2.79 and 1.30 $mg{\cdot}g^{-1}$ for onion peel, corn silk and conventional synthesis, respectively.

Another biologically derived material which may help in the synthesis of nanomaterials would be bovine serum albumin which Kim et al. [163] reported for the synthesis of magnetic iron oxide (average size, ~40 nm). These nanocomposites were reported for the extraction of phosphate ions from water solution. They reported a maximum adsorbance capacity of 20.7 $mg{\cdot}g^{-1}$. It was observed that other anions such as a Cl^-, $NO_3{}^-$, $CO_3{}^{2-}$ and $SO_4{}^{2-}$ did not have a large effect on the level of phosphate adsorbed. It was also reported that the desorption of phosphate was accomplished through the use of basic salt solution and that so-treated particles can continue adsorbing phosphate for up to 5 cycles with a removal rate of 68% on the fifth cycle.

4.2. Biochar/Magnetic Nanocomposites

It is also of interest to see the effect on the further treatment of biologic materials before their use in the formation of composites. One such method would be the thermal treatment of plant material to form biochar which is already an effective material for the removal of various contaminants due to its large surface area and affinity for the adsorption of chemical species. For this reason, biochar has already been demonstrated as a useful material for the formation of nanocomposites (Table 9).

Table 9. Magnetic nanocomposites made with biochars.

Source of Biochar	MNP (Other nps)	Surface Area ($m^2\ g^{-1}$)	Contaminant	Method of Removal	Ref.
Palm fibers	nZVIs	574	Cd^{2+}, As^{3+}	Adsorption	[170]
Oakwood	nZVIs	10.97	Cr(VI)	Adsorption	[171]
Rice straw	nZVIs	392.8	Cr(VI) Trichlorobenzene	Adsorption reduction	[172,173]
Pine needles	Fe_3O_4	175.3	Ethylbenzene	Fenton catalysis	[174]
Sewage sludge	nZVI	44	Sb(III)	Adsorption	[175]
Sewage sludge	$CoFe_2O_4$	N/A	norfloxacin	PMS activation	[176]
Wheat straw	nZVIs	60.3	Cr(VI)	Adsorption	[177]
Corn stalk	$CoFe_2O_4$	664.8	Bisphenol A	PMS activation	[178]
Rice straw	$CoFe_2O_4$	150.7	Metolachlor	PMS activation	[179]

It was reported by Fang et al. [170] that palm fibers, when converted to biochar can be used as a support for the synthesis of zerovalent iron nanoparticles (size range, 40–60 nm). The biochar, which forms a structure similar to graphene was bound to iron nanoparticles. These composites were then tested for the removal of cadmium (Cd^{2+}) and arsenic (As^{3+}) ions from water. It was discovered that while the biochar alone was a poor adsorbent of As^{3+} and Cd^{2+} and zerovalent iron shows limited ability when working together the adsorbance capacity of the nanocomposites increases to 30 $mg{\cdot}g^{-1}$ and 324 $mg{\cdot}g^{-1}$ for Cd^{2+} and As^{3+} respectively. They also observed that when the two ions were present together at pH of either 4 or 7 there was an increase in the amount of both ions adsorbed compared to the ions on their own and this indicates that this nanocomposite is an effective adsorbent for these two ions together. The usefulness of this nanocomposite was tested on samples of irrigation water. From an estimated 2 $mg{\cdot}L^{-1}$ of both contaminants at pH 6.5, 0.2 $g{\cdot}L^{-1}$ of the nanocomposite was able to reduce the concentration of Cd^{2+} by more than 95% and of As^{3+} by 100% in 30 min. Biochar from oakwood was also reported by Yang et al. [171] for the synthesis of nZVIs (size range, 90–200 nm) in the presence of tea phenols. The resulting composite was observed to remove close to 99% of a 50 $mg{\cdot}L^{-1}$ Cr(VI) solution. Other examples of biochar stabilizing nZVIs (size range, 30–50 nm) have been reported by Qian et al. who tested this materials for the degradation of trichlorobenzene [173,180] and Cr(VI) ions [172,181] from water resources. In all of these cases, modifications in the method for production of the biochar increased the rate of removal of the contaminant. Biochar was also used by Chen et al. [174] for the generation of a magnetite (average size, ~40 nm) composite which was demonstrated to degrade over 96% of a 0.1 $mmol{\cdot}L^{-1}$ solution of ethylbenzene in the presence of 2 $mmol{\cdot}L^{-1}$ H_2O_2. The magnetite nanoparticles communicate electronically through the biochar (Figure 9). It was determined the biochar structure aided in the production of reactive oxygen radicals which catalyzed the degradation of organic species in water.

Huang et al. [175] also reported the synthesis of nZVIs (average size, 30 nm) with biochar sourced from sewage sludge. This composite, which was derived from waste, showed a strong affinity for antimonite (Sb III) ions with a max adsorption capacity of 160.40 $mg{\cdot}g^{-1}$ at pH 4.8. They indicated that the process of adsorption occurred through complexation. Waste sludge was also utilized by Ding et al. [176] who used it as a support for growing $CoFe_2O_4$ nanoparticles (average size, <50 nm) through a solvothermal synthesis. These were then used for catalytic oxidation with PMS in order to remove the antibiotic norfloxacin from water. They report that almost all of a 10 $mg{\cdot}L^{-1}$ solution of the antibiotic can be degraded in 60 min. The presence of ions like chloride had a complicated effect on the degradation reaction with low concentrations inhibiting the reaction but higher concentrations showing an increase while carbonates only inhibit with increased concentration and nitrate has no major effect. Sludge can also be the source of the raw material for the formation of novel nanomaterials as reported by Wang et al. [182] who generated iron cobalt silicon dioxide nanomaterials (size range, 150–200 nm) through solvothermal treatment of waste sludge from drinking water treatment. This composite was tested for the activation of PMS and the treatment of ciprofloxacin. Up to 98% removal was reported in 10 min. Wheat straw was the source of the biochar that was used by Liu et al. [170] for supporting nZVIs (average size, ~100 nm) with carboxymethyl cellulose as an additional complexing agent. These nanocomposites were tested for the removal of Cr(VI) and demonstrated close to 100% removal of a 100 $mg{\cdot}L^{-1}$ solution of Cr through the addition of 1.25 $g{\cdot}L^{-1}$ of composite at pH 5.6 over 18 h with a q_m of 112.5 $mg{\cdot}g^{-1}$.

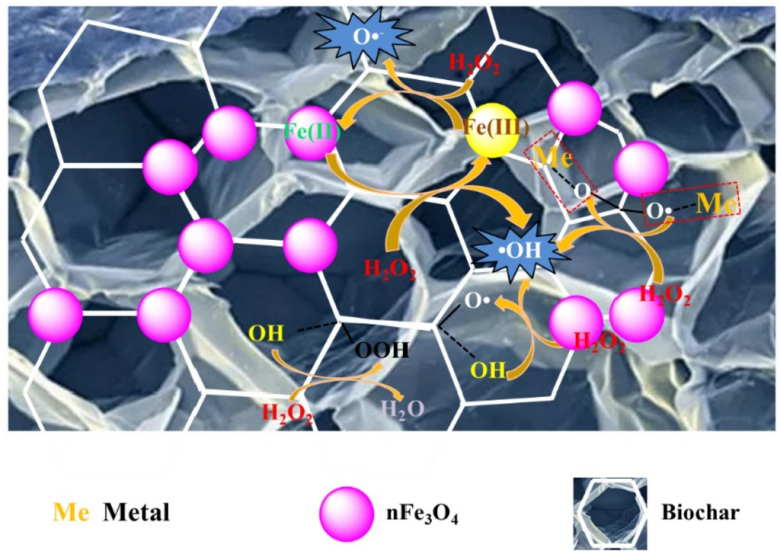

Figure 9. Proposed mechanism for ROSs generation in the nFe_3O_4/BC500 with activated H_2O_2. Reprinted from Chen et al. [174] with permission from Elsevier.

Corn stalk sourced biochar was used by Liu et al. [178] for the synthesis of $CoFe_2O_4$ nanoparticles (average size, ~100 nm) that were then used as activation catalysts with PMS for the oxidative degradation of bisphenol A and other common organic contaminant species (Figure 10). It was determined that the combination of biochar and cobalt ferrite was very effective for the removal of contaminants. Of a 10 $mg{\cdot}L^{-1}$ solution of bisphenol A, 100% was degraded in 8 min. Additional work was done on tartrazine, p-hydroxybenzoic acid, sulfadiazine and phenol and they showed values for degradation between 72% for p-Hydroxybenzoic acid and 98% for sulfadiazine. The degradation of bisphenol A was also performed in water from natural sources like rivers which demonstrated an increased time for full degradation of the contaminant. This reduction in performance is believed to be due to the presence of Cl^- and HCO_3^- ions in solution that are known to interfere in the catalytic process. It would be important to be aware of these environmental factors before considering the use of such composites in the field.

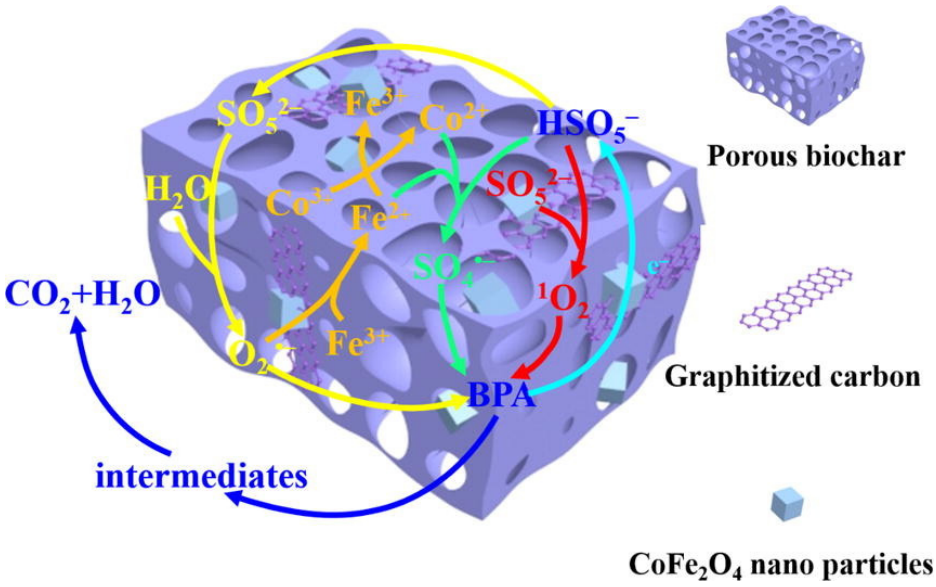

Figure 10. General scheme for the interactions between $CoFe_2O_4$ nanoparticles on graphene-like biochar for the activation of PMS for the degradation of bisphenol A. Reprinted from Liu et al. [178] with permission of Elsevier.

Rice straw was reported as the source for biochar by Cai et al. [179] who impregnated a biochar with cobalt ferrite nanoparticles using a robust impregnation and pyrolysis method. The resulting composite was used to catalyze the activation of PMS and subsequent degradation of the herbicide metolachlor. For composites pyrolyzed at 800 °C removal efficiencies of greater than 80% of a 10 $mg \cdot L^{-1}$ herbicide solution was sustained even after 3 cycles of use.

4.3. Microbial/Magnetic Nanocomposites

While natural products and their derivatives may be useful for the formation of nanocomposites, the use of full organisms especially microorganisms can be useful. Microbes are functional in their form and contain many chemical species that can perform processes that may be usefully harnessed. This can occur with both processed and live microbes as shown (Table 10).

Table 10. Microorganisms used in the formation of magnetic nanocomposites.

Organism	Processing	MNP	Surface Area ($m^2\ g^{-1}$)	Contaminant	Removal Mechanism	Ref.
Aspergillus niger	Deactivated	Reduced iron	N/A	Cr(VI)	Adsorption	[183]
Brewer's yeast	Dried	Fe_3O_4	67	Oil	Adsorption	[184,185]
Bacillus cereus SO-14	Dried and ground	γ-Fe_2O_3	N/A	U and Th ions	Adsorption	[186]
Ulva prolifera	Crushed	S–nZVI	56.3	BrO_3^-	Adsorption	[187]
Shewanella putrefaciens	None	nZVI	N/A	Pentachlorophenol	Reduction	[188]
Aeromonas hydrophila	None	nZVI	N/A	Cr(VI)	Reduction	[189]
Pleurotus ostreatus	Dried and powdered	iron oxide	N/A	Ni^{2+} + Pb^{2+}	Adsorption	[190]
Var. spp.	None	Fe_3O_4	N/A	Di-(2-ethylhexyl) phthalate	Reduction	[191]

An interesting composite of deactivated *A. niger* fungal hyphae with magnetic reduced iron nanoparticles with graphene oxide has been reported by Wang et al. [183]. These composites were tested for the removal of Cr(VI) ions from water and demonstrated adsorbance values of up to 58 $mg \cdot g^{-1}$ which were higher than the values observed for the untreated fungus and GO. A possible mechanism for this increase was elucidated through FTIR and TGA analysis which indicated a slight reduction in the presence of iron in the composite after adsorption. The authors of the study propose Cr(VI) ions bind to the surface of the zerovalent iron in the nanomaterials which then reduce the Cr(VI) to Cr(III) trapping it as a layer of chromic ferrite on the particles. As this was noted to only occur in the surface, there was no significant increase in mass.

Yeast cells acquired from the brewing industry were used by Labuto et al. [184] who used a dried yeast biomass suspension to generate stabilized magnetite nanoparticles (size range, 12–14 nm). These composite particles showed good activity for the removal of different types of oil from water demonstrating maximum removal values of 3522 ± 118 $g \cdot kg^{-1}$, 2841 ± 280 $g \cdot kg^{-1}$ and 2157 ± 281 $g \cdot kg^{-1}$ for new motor oil, mixed used motor oil and P28 API oil, respectively. In addition, Labuto et al. [185] examined the effectiveness of yeast stabilized magnetite nanoparticles compared to magnetite made with cork powder and bare magnetite nanoparticles for the removal of oil from deionized and sea water. Both the yeast and cork stabilized nanoparticles displayed better removal performance compared to the bare nanoparticles in terms of mass retained, but there may be issues with the retention of water with the presence of the nanocomposites which skewed the results. It was also found that oil API number was a greater determinant of removal performance compared to water salinity or the use of passive floating or vortex to mix the oil and nanocomposite.

In a similar report, dried and ground bacterial cells were immobilized on magnetic nanoparticles by Sen et al. [186] In this work, the thermophilic *Bacillus cereus* SO-14 was bound to γ-Fe_2O_3 nanoparticles and then placed into an magnetic solid phase extraction column and used to concentrate uranium and thorium ions from water in order to aid ICP-OES analysis. Using this flow system close to 100% recovery of both metals ions were achieved from a solution of 10 ng·L^{-1} with a concentration factor of close to 100.

Crushed samples of the alga *Ulva prolifera* was used by Wu et al. [187] as a starting material for the synthesis of S–nZVIs through a solvothermal synthesis which were then demonstrated to be effective in the removal of Bromate (BrO_3^-), a disinfection byproduct. Up to 98% removal of a 100 μg·L^{-1} bromate solution was reported after 48 min with 85% removal still occurring after 5 cycles of use and reuse.

Extracellular polymeric substances (EPS), a series of materials that are extruded by bacteria and which can conduct electricity while preventing the entry of oxygen, was investigated as a stabilization agent for nZVIs by Yang et al. [164]. It was determined that this nanocomposite had a high degree of adsorption capacity for antimony (Sb) (V) ions from water demonstrating a maximum efficiency of 202 mg·g^{-1} at pH 5. With the use of EPS, the nanocomposite showed greater stability with respect to the presence of oxygen than has previously determined for zerovalent iron. This helps the engaging of the nZVI mediated Fenton reaction for the reduction of Sb(V) (Figure 11).

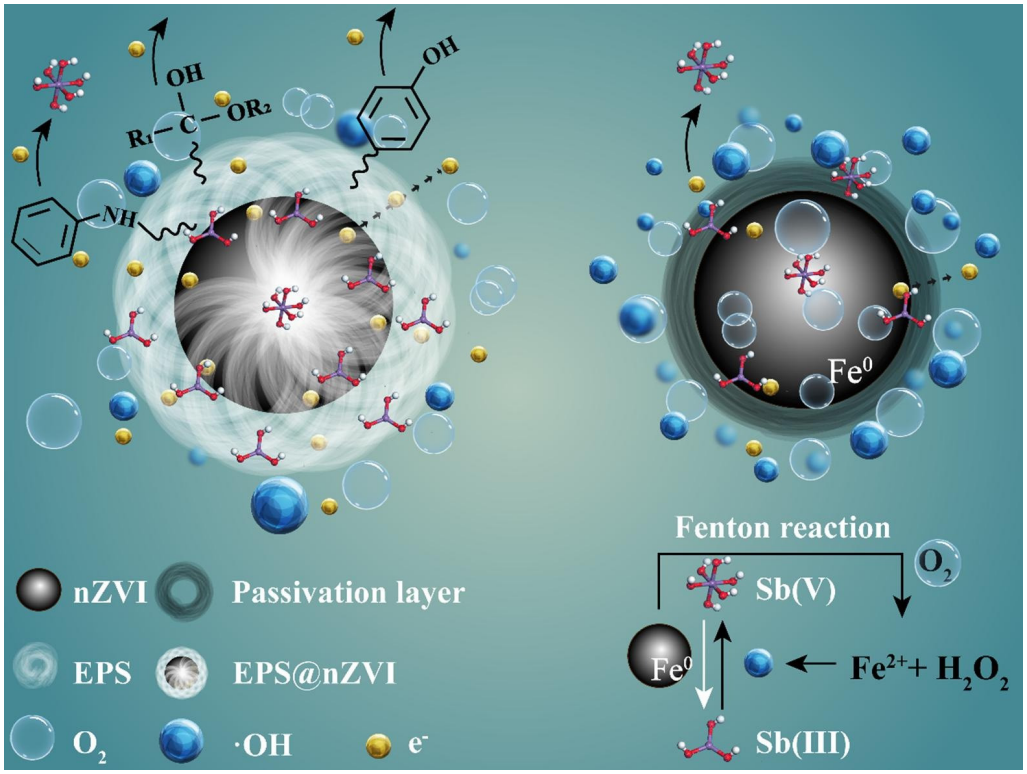

Figure 11. Effect of extracellular polymeric substances (EPS) on the removal of Sb(V) ions from solution by zerovalent iron particles (nZVIs). (left) Passivated nZVI shows much higher levels of removal. Reprinted from Yang-Yang et al. [164] with permission from Elsevier.

The EPS extracted from anaerobic sludge was used by Shen et al. [165] to link to S–nZVI particles that could then catalyze the reduction of nitrobenzene to aniline. It was demonstrated that not only could the presence of S–nZVI enhance the rate of reduction of nitrobenzene, but it improved the stability of the bio system with improved electron transfer between the different strains of bacteria in the sludge and consequent increases in fermentation, electroactivity and methanogenesis, other useful processes for waste treatment. Considering the cost of these nanomaterials, the addition of a S–nZVI may be a cost-effective method for improving the efficiency of anaerobic bioprocessing of waste waters.

Live anaerobic bacteria of the species *Alcaligenes eutrophus* was bound to nZVI particles (average size, 50 nm) by An et al. [192] who reported that these nanocomposites demonstrate better stability for transport and against sedimentation compared to unbound nanoparticles. When the observed catalytic activity of zero-valent iron nanoparticles is considered this improved stability may be important for the use of this class of materials in the remediation of water. Another species of bacteria that demonstrated an interaction with nZVI was *Shewanella putrefaciens* CN32 which were reported by Yang et al. [188] to greatly increase the reduction of pentachlorophenol by these nanoparticles when deposited on a biochar base (size range, 40–50 nm). The bacterial reduced the nanoparticles through the biochar and prevented loss of activity through aging. Up to 97.6% degradation of the organic contaminant can be achieved in this way. Xie et al. [189] reported similar effects with *Aeromonas hydrophila* directly reducing nZVIs and activating the surface of the nanoparticles for the reduction of Cr(VI).

Other live bacteria were used by Xu et al. [191] who isolated bacterial strains resistant to Di-(2-ethylhexyl) phthalate (DEHP) from bacterial sludge and then used them in conjunction with nanomagnetite (Fe_3O_4) coated on biochar to degrade this environmental toxin with over 92% degradation reported over 24 days incubation.

More advanced organisms were also reported for the generation of nanocomposites. Kılınç et al. [190] reported the use of powdered samples of a common edible oyster mushroom, *Pleurotus ostreatus*, in the synthesis of iron oxide nanoparticles which were then demonstrated as bio-adsorbents for Ni^{2+} and Pb^{2+} ions from water. Maximum adsorbance capacities were reported of 28.6 and 32.1 $mg \cdot g^{-1}$ for Ni^{2+} and Pb^{2+}, respectively.

4.4. Conclusions

In conclusion, three distinct classes of biological material magnetic nanocomposites have been discussed in this review. First, there are biopolymer composites. These nanocomposites primarily demonstrated adsorption activity though the presence of iron species in magnetic component permitted the catalysis of the Fenton reaction under certain conditions. Biochar, which was sourced from many different biologic products and waste materials was used to form magnetic composites which demonstrated both adsorption behavior and catalytic activity. Finally, microorganisms demonstrated effectiveness as the basis of magnetic nanocomposites. When generated using processed microorganisms, good adsorption behavior was reported while, interestingly, in presence of nZVIs particles live bacteria could aid in the reduction of contaminant species at greater efficiency than free particles. Due to their good performance and generally wide availability biological materials will likely have an increasing presence in this field in the future.

5. Key Concepts for the Future

From this quick survey of the most recent literature, the following general conclusions can be reached:

The field of magnetic nanomaterials for application in the remediation of water resources is a highly active area of research. With an ever-increasing number of papers on this theme being published each year and no sign of interest in the field waning, we should expect increasing developments in this field long into the future.

(1) The use of nanomaterials enables a high degree of economy for the use of materials for the removal of various contaminants from water. Within the course of the review, we have highlighted examples of near-to- or above-unity-adsorption of contaminants such as have been reported for layered double hydroxides [75] and layered double oxides [74] containing composites, nickel, magnesium-and-zinc-ferrite nanoparticles [40], and chitosan with tin oxide [154] all of which can adsorb a large quantity of contaminants in a short period of time. Linked with the ability to be retained with a magnetic field and then reused over multiple cycles, it appears that only a small quantity of this class of nanomaterial would be necessary for remediating a large volume of water. This would be beneficial both environmentally and economically, as less material would be

necessarily dispersed into water sources in order to remove contamination, and less raw material would be needed to perform contaminant removal. A similar observation may be made for the catalytic nanomaterials reported that could serve to degrade contaminants either singly or in the presence of oxidizing agents such as hydrogen peroxide [37] and oxygen [105] or reducing agents such as borohydride [139,141].

(2) We see an increasing usage of biological materials, both processed and unprocessed, in the generation of novel nanocomposite materials. The use of biologic materials has certain benefits, as they may be designed for the specific application to which the composite has been produced, for example the transfer of electrons between nZVIs and substrate molecules [165]. Enlisting biological materials in the formation of nanocomposites enables us to use the evolution-perfected properties of these materials in our desired materials.

(3) We also observe the formation of nanocomposites using various forms of waste material (Table 11). Through the use of waste materials, it is possible to not only to reduce the effect of contamination on water resources, but also to reduce the amount of waste being generated by the industrial source of the feedstock. This can be an important contribution to the long-term goal of bringing about a zero-waste economy.

Table 11. Examples of magnetic nanocomposites made using waste materials.

Waste Source	Material Generated Using Waste	Resulting Composite	Contaminant	Ref.
E-waste	V_2O_5	$ZnFe_2O_4$@V_2O_5	BTEX	[132]
Water treatment waste sludge	Sludge-based activated carbon	Mg–Fe LDH/SBAC MgFe composite	NO_3^- and PO_4^{3-}	[81]
Magnetic fly ash	C@magnetic fly ash	chitosan/polydopamine @C@magnetic fly ash	Ag^+	[169]
Orange fruit residue	Pectin based stabilizer	Pectin stabilized $CoFe_2O_4$	Oil	[157]
Wheat straw	Biochar	Biochar-CMC-nZVI	Cr(VI)	[177]
Coal fly ash	Na-X Zeolite	Magnetic nanoparticle/ Zeolite composite	Cd^{2+} + Pb^{2+}	[87]
Iron oxide powders from mineral processing	Raw-waste iron oxide	Fe_2O_3@TiO_2 composite	Water-soluble dyes	[131]

However, there are issues which also need be addressed before these materials are in widespread use. These include,

1. Enabling synthesis methods for the reliable generation of magnetic nanomaterials. This review demonstrates many different types of magnetic nanomaterial which have been prepared using many different methods. Most these reports are preliminary and there will be a long time required to fully optimize the synthesis protocols for the use of these new technologies on the industrial scale;
2. While promising, figures for the reuse of the reported nanomaterials still indicates a loss of material through repeated use. To better fulfill the promise of these new class of material it will be necessary to ensure complete retention of the nanomaterial and its full regeneration in a rapid and economical way;
3. Finally, as stated in the introduction, nanomaterials can be contaminants either as full particles on their own, or as a source of breakdown products such as metal ions or organic molecules that can be hazardous to human health. This means that if there is a loss during use, then this potential method for remediating water can instead be a source of contamination. As such, before the widespread use of these novel materials for the remediation of water protocols must be developed to limit the potential risk to human health and the environment and to prevent accidental release.

In closing, the development of novel nanoparticles and composite materials is a highly active area of research which has incredible potential for the remediation and continued utilization of water resources going into the future.

Funding: This research received no external funding.

Conflicts of Interest: The author declares no conflict of interest.

References

1. Glieck, P.H. *Water in Crisis, A. Guide to the World's Fresh Water Resources*; Oxford University Press: Oxford, UK, 1993.
2. Salgot, M.; Huertas, E.; Weber, S.; Dott, W.; Hollender, J. Wastewater reuse and risk: Definition of key objectives. *Desalination* **2006**, *187*, 29–40. [CrossRef]
3. Boretti, A.; Rosa, L. Reassessing the projections of the World Water Development Report. *NPJ Clean Water* **2019**, *2*, 15. [CrossRef]
4. Lyu, S.; Chen, W.; Zhang, W.; Fan, Y.; Jaio, W. Wastewater reclamation and reuse in China: Opportunities and challenges. *J. Environ. Sci.* **2016**, *39*, 86–96. [CrossRef]
5. Hlongwane, G.N.; Sekoai, P.T.; Meyyappan, M.; Moothi, K. Simultaneous removal of pollutants from water using nanoparticles: A shift from single pollutant control to multiple pollutant control. *Sci. Total Environ.* **2019**, *656*, 808–833. [CrossRef]
6. Flanagan, P.J. *Parameters of Water Quality Interpretation and Standards*; The Environmental Protection Agency: Dublin, Ireland, 2001.
7. Xu, J.-Z.; Dai, L.; Wu, B.; Ding, T.; Zhu, J.-J.; Lin, H.; Chen, H.-L.; Shen, C.-Y.; Jiang, Y. Determination of methylene blue residues in aquatic products by liquid chromatography-tandem mass spectrometry. *J. Sep. Sci.* **2009**, *32*, 4193–4199. [CrossRef]
8. Diagnostics, P.-L. Crystal Violet MSDS. 2017. Available online: https://www.pro-lab.com/wp-content/uploads/2016/11/Crystal-Violet-SDS780-EN.pdf (accessed on 4 September 2020).
9. Compound Summary 2,3-Dichlorophenol. In PubChem. 2005. Available online: https://pubchem.ncbi.nlm.nih.gov/compound/dichlorophenol (accessed on 4 September 2020).
10. Liu, B.; Liu, J. Sensors and biosensors based on metal oxide nanomaterials. *TrAC Trends Anal. Chem.* **2019**, *121*, 115690. [CrossRef]
11. Wang, H.; Le-Van, Q.; Aassime, A.; Roux, X.L.; Charra, F.; Chauvin, N.; Degiron, A. Electroluminescence of Colloidal Quantum Dots in Electrical Contact with Metallic Nanoparticles. *Adv. Opt. Mater.* **2018**, *6*, 1700658. [CrossRef]
12. Nasir, A.; Kausar, A.; Younus, A. A Review on Preparation, Properties and Applications of Polymeric Nanoparticle-Based Materials. *Polym. Plast. Technol. Eng.* **2015**, *54*, 325–341. [CrossRef]
13. Li, Z.; Ji, S.; Liu, Y.; Cao, X.; Tian, S.; Chen, Y.; Niu, Z.; Li, Y. Well-Defined Materials for Heterogeneous Catalysis: From Nanoparticles to Isolated Single-Atom Sites. *Chem. Rev.* **2020**, *120*, 623–682. [CrossRef]
14. Soares, S.; Sousa, J.; Pais, A.; Vitorino, C. Nanomedicine: Principles, Properties, and Regulatory Issues. *Front. Chem.* **2018**, *6*, 360. [CrossRef]
15. Tahoon, M.A.; Siddeeg, S.M.; Salem Alsaiari, N.S.; Mnif, W.; Ben Rebah, F. Effective Heavy Metals Removal from Water Using Nanomaterials: A Review. *Processes* **2020**, *8*, 645. [CrossRef]
16. Xue, X.; Cheng, R.; Shi, L.; Ma, Z.; Zheng, X. Nanomaterials for water pollution monitoring and remediation. *Environ. Chem. Lett.* **2017**, *15*, 23–27. [CrossRef]
17. Ali, I. New Generation Adsorbents for Water Treatment. *Chem. Rev.* **2012**, *112*, 5073–5091. [CrossRef]
18. Ersan, G.; Apul, O.G.; Perreault, F.; Karanfil, T. Adsorption of organic contaminants by graphene nanosheets: A review. *Water Res.* **2017**, *126*, 385–398. [CrossRef] [PubMed]
19. Lata, S.; Singh, P.K.; Samadder, S.R. Regeneration of adsorbents and recovery of heavy metals: A review. *Int. J. Environ. Sci. Technol.* **2015**, *12*, 1461–1478. [CrossRef]
20. Qian, J.; Gao, X.; Pan, B. Nanoconfinement-Mediated Water Treatment: From Fundamental to Application. *Environ. Sci. Technol.* **2020**, *54*, 8509–8526. [CrossRef]
21. Yin, Y.B.; Guo, S.; Heck, K.N.; Clark, C.A.; Coonrod, C.L.; Wong, M.S. Treating Water by Degrading Oxyanions Using Metallic Nanostructures. *ACS Sustain. Chem. Eng.* **2018**, *6*, 11160–11175. [CrossRef]

22. Lee, J.; von Gunten, U.; Kim, J.-H. Persulfate-Based Advanced Oxidation: Critical Assessment of Opportunities and Roadblocks. *Environ. Sci. Technol.* **2020**, *54*, 3064–3081. [CrossRef]
23. Buchman, J.T.; Hudson-Smith, N.V.; Landy, K.M.; Haynes, C.L. Understanding Nanoparticle Toxicity Mechanisms To Inform Redesign Strategies To Reduce Environmental Impact. *Acc. Chem. Res.* **2019**, *52*, 1632–1642. [CrossRef]
24. Lu, F.; Astruc, D. Nanocatalysts and other nanomaterials for water remediation from organic pollutants. *Coord. Chem. Rev.* **2020**, *408*, 213180. [CrossRef]
25. García Doménech, N.; Purcell-Milton, F.; Gun'ko, Y.K. Recent progress and future prospects in development of advanced materials for nanofiltration. *Mater. Today Commun.* **2020**, *23*, 100888. [CrossRef]
26. Kirkegaard, P.; Hansen, S.F.; Rygaard, M. Potential exposure and treatment efficiency of nanoparticles in water supplies based on wastewater reclamation. *Environ. Sci. Nano* **2015**, *2*, 191–202. [CrossRef]
27. Beveridge, J.S.; Stephens, J.R.; Williams, M.E. The Use of Magnetic Nanoparticles in Analytical Chemistry. *Annu. Rev. Anal. Chem.* **2011**, *4*, 251–273. [CrossRef] [PubMed]
28. Govan, J.; Gun'ko, Y.K. Recent Advances in the Application of Magnetic Nanoparticles as a Support for Homogeneous Catalysts. *Nanomaterials* **2014**, *4*, 222–241. [CrossRef] [PubMed]
29. Xiao, D.; Lu, T.; Zeng, R.; Bi, Y. Preparation and highlighted applications of magnetic microparticles and nanoparticles: A review on recent advances. *Microchim. Acta* **2016**, *183*, 2655–2675. [CrossRef]
30. Abdel Maksoud, M.I.A.; Elgarahy, A.M.; Farrell, C.; Al-Muhtaseb, A.H.; Rooney, D.W.; Osman, A.I. Insight on water remediation application using magnetic nanomaterials and biosorbents. *Coord. Chem. Rev.* **2020**, *403*, 213096. [CrossRef]
31. Peralta, M.E.; Ocampo, S.; Funes, I.G.; Onaga Medina, F.; Parolo, M.E.; Carlos, L. Nanomaterials with Tailored Magnetic Properties as Adsorbents of Organic Pollutants from Wastewaters. *Inorganics* **2020**, *8*, 24. [CrossRef]
32. Kumari, P.; Kumar, S.; Singhal, A. Chapter 29-Magnetic nanoparticle-based nanocontainers for water treatment. In *Micro and Nano Technologies*; Nguyen-Tri, P., Do, T.-O., Nguyen, T.-S.N., Eds.; Elsevier: Amsterdam, The Netherlands, 2020; pp. 487–498.
33. Singh, H.; Bhardwaj, N.; Arya, S.K.; Khatri, M. Environmental impacts of oil spills and their remediation by magnetic nanomaterials. *Environ. Nanotechnol. Monit. Manag.* **2020**, *14*, 100305. [CrossRef]
34. Kharisov, B.I.; Rasika Dias, H.V.; Kharissova, O.V.; Manuel Jiménez-Pérez, V.; Olvera Pérez, B.; Muñoz Flores, B. Iron-containing nanomaterials: Synthesis, properties, and environmental applications. *RSC Adv.* **2012**, *2*, 9325–9358. [CrossRef]
35. Singh, P.; Sharma, K.; Hasija, V.; Sharma, V.; Sharma, S.; Raizada, P.; Singh, M.; Saini, A.K.; Hosseini-Bandegharaei, A.; Thakur, V.K. Systematic review on applicability of magnetic iron oxides–integrated photocatalysts for degradation of organic pollutants in water. *Mater. Today Chem.* **2019**, *14*, 100186. [CrossRef]
36. Fato, F.P.; Li, D.-W.; Zhao, L.-J.; Qiu, K.; Long, Y.-T. Simultaneous Removal of Multiple Heavy Metal Ions from River Water Using Ultrafine Mesoporous Magnetite Nanoparticles. *ACS Omega* **2019**, *4*, 7543–7549. [CrossRef] [PubMed]
37. Li, X.; Li, J.; Shi, W.; Bao, J.; Yang, X. A Fenton-Like Nanocatalyst Based on Easily Separated Magnetic Nanorings for Oxidation and Degradation of Dye Pollutant. *Materials* **2020**, *13*, 332. [CrossRef] [PubMed]
38. Yang, J.-C.E.; Lin, Y.; Peng, H.-H.; Yuan, B.; Dionysiou, D.D.; Huang, X.-D.; Zhang, D.-D.; Fu, M.-L. Novel magnetic rod-like Mn-Fe oxycarbide toward peroxymonosulfate activation for efficient oxidation of butyl paraben: Radical oxidation versus singlet oxygenation. *Appl. Catal. B Environ.* **2020**, *268*, 118549. [CrossRef]
39. Ma, C.; Liu, F.-Y.; Wei, M.-B.; Zhao, J.-H.; Zhang, H.-Z. Synthesis of Novel Core-Shell Magnetic Fe_3O_4@C Nanoparticles with Carboxyl Function for Use as an Immobilisation Agent to Remediate Lead-Contaminated Soils. *Pol. J. Environ. Stud.* **2020**, *29*, 2273–2283. [CrossRef]
40. Yu, L.; Li, Y.; Pan, S.; Huang, W.; Liu, R. Adsorption Mechanisms and Electrochemical Properties of Methyl Blue onto Magnetic NixMgyZn(1-x-y)Fe_2O_4 Nanoparticles Fabricated Via the Ethanol-Assisted Combustion Process. *Water Air Soil Pollut.* **2020**, *231*, 316. [CrossRef]
41. Iqbal, A.; Jacob, J.; Mahmood, A.; Mehboob, K.; Mahmood, K.; Ali, A.; Bukhari, T.-H.; Adrees, M.; Adrees, M.; Ahmad, M. Synthesis and characterization of Zn–Mn–Fe nano oxide composites for the degradation of reactive yellow 15 dye. *Phys. B Condens. Matter* **2020**, *588*, 412210. [CrossRef]
42. Liu, Y.; Yu, H.; Zou, D. One-Step Synthesis of Metal-Modified Nanomagnetic Materials and Their Application in the Removal of Chlortetracycline. *ACS Omega* **2020**, *5*, 5116–5125. [CrossRef]

43. Zhang, H.; Li, C.; Lyu, L.; Hu, C. Surface oxygen vacancy inducing peroxymonosulfate activation through electron donation of pollutants over cobalt-zinc ferrite for water purification. *Appl. Catal. B Environ.* **2020**, *270*, 118874. [CrossRef]
44. Vasiljevic, Z.Z.; Dojcinovic, M.P.; Krstic, J.B.; Ribic, V.; Tadic, N.B.; Ognjanovic, M.; Auger, S.; Vidic, J.; Nikolic, M.V. Synthesis and antibacterial activity of iron manganite ($FeMnO_3$) particles against the environmental bacterium Bacillus subtilis. *RSC Adv.* **2020**, *10*, 13879–13888. [CrossRef]
45. Abdel Maksoud, M.I.A.; El-Sayyad, G.S.; El-Khawaga, A.M.; Abd Elkodous, M.; Abokhadra, A.; Elsayed, M.A.; Gobara, M.; Soliman, L.I.; El-Bahnasawy, H.H.; Ashour, A.H. Nanostructured Mg substituted Mn-Zn ferrites: A magnetic recyclable catalyst for outstanding photocatalytic and antimicrobial potentials. *J. Hazard. Mater.* **2020**, *399*, 123000. [CrossRef]
46. Abou Hammad, A.B.; Hemdan, B.A.; El Nahrawy, A.M. Facile synthesis and potential application of Ni0.6Zn0.4Fe2O4 and Ni0.6Zn0.2Ce0.2Fe2O4 magnetic nanocubes as a new strategy in sewage treatment. *J. Environ. Manag.* **2020**, *270*, 110816. [CrossRef] [PubMed]
47. Liu, J.; Liu, A.; Wang, W.; Li, R.; Zhang, W.-X. Feasibility of nanoscale zero-valent iron (nZVI) for enhanced biological treatment of organic dyes. *Chemosphere* **2019**, *237*, 124470. [CrossRef] [PubMed]
48. Qiao, J.; Guo, Y.; Dong, H.; Guan, X.; Zhou, G.; Sun, Y. Activated peroxydisulfate by sulfidated zero-valent iron for enhanced organic micropollutants removal from water. *Chem. Eng. J.* **2020**, *396*, 125301. [CrossRef]
49. Guan, X.; Du, X.; Liu, M.; Qin, H.; Qiao, J.; Sun, Y. Enhanced trichloroethylene dechlorination by carbon-modified zero-valent iron: Revisiting the role of carbon additives. *J. Hazard. Mater.* **2020**, *394*, 122564. [CrossRef] [PubMed]
50. Singh, R.; Bhateria, R. Experimental and Modeling Process Optimization of Lead Adsorption on Magnetite Nanoparticles via Isothermal, Kinetics, and Thermodynamic Studies. *ACS Omega* **2020**, *5*, 10826–10837. [CrossRef] [PubMed]
51. Amos-Tautua, B.M.; Fakayode, O.J.; Songca, S.P.; Oluwafemi, O.S. Effect of synthetic conditions on the crystallinity, porosity and magnetic properties of gluconic acid capped iron oxide nanoparticles. *Nano-Struct. Nano-Objects* **2020**, *23*, 100480. [CrossRef]
52. Powell, C.D.; Atkinson, A.J.; Ma, Y.; Marcos-Hernandez, M.; Villagran, D.; Westerhoff, P.; Wong, M.S. Magnetic nanoparticle recovery device (MagNERD) enables application of iron oxide nanoparticles for water treatment. *J. Nanopart. Res.* **2020**, *22*, 48. [CrossRef]
53. Di Iorio, E.; Colombo, C.; Cheng, Z.; Capitani, G.; Mele, D.; Ventruti, G.; Angelico, R. Characterization of magnetite nanoparticles synthetized from Fe(II)/nitrate solutions for arsenic removal from water. *J. Environ. Chem. Eng.* **2019**, *7*, 102986. [CrossRef]
54. Nejad, S.B.; Mohammadi, A. Epoxy-Triazinetrione-Functionalized Magnetic Nanoparticles as an Efficient Magnetic Nanoadsorbent for the Removal of Malachite Green and Pb(II) from Aqueous Solutions. *J. Chem. Eng. Data* **2020**, *65*, 2731–2742. [CrossRef]
55. Feng, J.; Zhang, J.; Song, W.; Liu, J.; Hu, Z.; Bao, B. An environmental-friendly magnetic bio-adsorbent for high-efficiency Pb(II) removal: Preparation, characterization and its adsorption performance. *Ecotoxicol. Environ. Saf.* **2020**, *203*, 111002. [CrossRef]
56. H Kamel, A.; Hassan, A.A.; Amr, A.E.-G.E.; El-Shalakany, H.H.; Al-Omar, A.M. Synthesis and Characterization of CuFe2O4 Nanoparticles Modified with Polythiophene: Applications to Mercuric Ions Removal. *Nanomaterials* **2020**, *10*, 586. [CrossRef] [PubMed]
57. Kim, J.-H.; Kim, S.-M.; Yoon, I.-H.; Kim, I. Application of polyethylenimine-coated magnetic nanocomposites for the selective separation of Cs-enriched clay particles from radioactive soil. *RSC Adv.* **2020**, *10*, 21822–21829. [CrossRef]
58. Villa, S.; Riani, P.; Soggia, F.; Magi, E.; Canepa, F. Thiol-functionalized magnetic nanoparticles for static and dynamic removal of Pb(II) ions from waters. *J. Nanopart. Res.* **2019**, *21*, 44. [CrossRef]
59. Tavares, D.S.; Lopes, C.B.; Almeida, J.C.; Vale, C.; Pereira, E.; Trindade, T. Spinel-type ferrite nanoparticles for removal of arsenic(V) from water. *Environ. Sci. Pollut. Res.* **2020**, *27*, 22523–22534. [CrossRef]
60. Cai, C.; Kang, S.; Xie, X.; Liao, C.; Duan, X.; Dionysiou, D.D. Efficient degradation of bisphenol A in water by heterogeneous activation of peroxymonosulfate using highly active cobalt ferrite nanoparticles. *J. Hazard. Mater.* **2020**, *399*, 122979. [CrossRef] [PubMed]

61. Yang, Y.; Zhang, Y.; Wang, Z. Adsorption characteristics and electrochemical performance of reactive red onto magnetic MgFe2O4 nanoparticles prepared via a facile alcohol combustion process. *J. Sol-Gel Sci. Technol.* **2020**, *93*, 535–545. [CrossRef]
62. Yu, R.; Zhao, J.; Zhao, Z.; Cui, F. Copper substituted zinc ferrite with abundant oxygen vacancies for enhanced ciprofloxacin degradation via peroxymonosulfate activation. *J. Hazard. Mater.* **2020**, *390*, 121998. [CrossRef]
63. Oh, D.; Lee, C.-S.; Kang, Y.-G.; Chang, Y.-S. Hydroxylamine-assisted peroxymonosulfate activation using cobalt ferrite for sulfamethoxazole degradation. *Chem. Eng. J.* **2020**, *386*, 123751. [CrossRef]
64. Kaur, R.; Bakshi, M.S. Mechanistic Aspects of Simultaneous Extraction of Ag and Au Nanoparticles across Aqueous–Organic Interface by Surface Active Iron Oxide Nanoparticles. *Langmuir* **2020**, *36*, 7505–7516. [CrossRef]
65. Tian, H.; Liang, Y.; Yang, D.; Sun, Y. Characteristics of PVP–stabilised NZVI and application to dechlorination of soil–sorbed TCE with ionic surfactant. *Chemosphere* **2020**, *239*, 124807. [CrossRef]
66. Guo, W.; Zhao, Q.; Du, J.; Wang, H.; Li, X.; Ren, N. Enhanced removal of sulfadiazine by sulfidated ZVI activated persulfate process: Performance, mechanisms and degradation pathways. *Chem. Eng. J.* **2020**, *388*, 124303. [CrossRef]
67. Zheng, H.; Ren, X.; Zhang, X.; Song, G.; Chen, D.; Chen, C. Mutual effect of U(VI) and phosphate on the reactivity of nanoscale zero-valent iron (nZVI) for their co-removal. *J. Mol. Liq.* **2020**, *297*, 111853. [CrossRef]
68. Wei, X.; Yin, H.; Peng, H.; Guo, Z.; Lu, G.; Dang, Z. Sulfidation enhanced reduction of polybrominated diphenyl ether and Pb(II) combined pollutants by nanoscale zerovalent iron: Competitive reaction between pollutants and electronic transmission mechanism. *Chem. Eng. J.* **2020**, *395*, 125085. [CrossRef]
69. Bhattacharjee, S.; Darwish, N.; Shanableh, A. Phosphate removal using nanoscale zerovalent iron: Impact of chitosan and humic acid. *J. Environ. Chem. Eng.* **2020**, *8*, 104131. [CrossRef]
70. Xu, W.; Hu, X.; Lou, Y.; Jiang, X.; Shi, K.; Tong, Y.; Xu, X.; Shen, C.; Hu, B.; Lou, L. Effects of environmental factors on the removal of heavy metals by sulfide-modified nanoscale zerovalent iron. *Environ. Res.* **2020**, *187*, 109662. [CrossRef]
71. Qin, H.; Yin, D.; Bandstra, J.Z.; Sun, Y.; Cao, G.; Guan, X. Ferrous ion mitigates the negative effects of humic acid on removal of 4-nitrophenol by zerovalent iron. *J. Hazard. Mater.* **2020**, *383*, 121218. [CrossRef]
72. Li, J.; Sun, Y.; Zhang, X.; Guan, X. Weak magnetic field enables high selectivity of zerovalent iron toward metalloid oxyanions under aerobic conditions. *J. Hazard. Mater.* **2020**, *400*, 123330. [CrossRef]
73. Fan, P.; Li, L.; Sun, Y.; Qiao, J.; Xu, C.; Guan, X. Selenate removal by Fe0 coupled with ferrous iron, hydrogen peroxide, sulfidation, and weak magnetic field: A comparative study. *Water Res.* **2019**, *159*, 375–384. [CrossRef]
74. Palza, H.; Delgado, K.; Govan, J. Novel magnetic CoFe2O4/layered double hydroxide nanocomposites for recoverable anionic adsorbents for water treatment. *Appl. Clay Sci.* **2019**, *183*, 105350. [CrossRef]
75. Shi, S.; Zhang, W.; Wu, H.; Li, Y.; Ren, X.; Li, M.; Liu, J.; Sun, J.; Yue, T.; Wang, J. In Situ Cascade Derivation toward a Hierarchical Layered Double Hydroxide Magnetic Absorbent for High-Performance Protein Separation. *ACS Sustain. Chem. Eng.* **2020**, *8*, 4966–4974. [CrossRef]
76. Abdullah, N.H.; Shameli, K.; Abdullah, E.C.; Abdullah, L.C. Low cost and efficient synthesis of magnetic iron oxide/activated sericite nanocomposites for rapid removal of methylene blue and crystal violet dyes. *Mater. Charact.* **2020**, *163*, 110275. [CrossRef]
77. Liu, Y.; Li, J.; Wu, L.; Shi, Y.; He, Q.; Chen, J.; Wan, D. Magnetic spent bleaching earth carbon (Mag-SBE@C) for efficient adsorption of tetracycline hydrochloride: Response surface methodology for optimization and mechanism of action. *Sci. Total Environ.* **2020**, *722*, 137817. [CrossRef] [PubMed]
78. Das, K.C.; Dhar, S.S. Removal of cadmium(II) from aqueous solution by hydroxyapatite-encapsulated zinc ferrite (HAP/$ZnFe_2O_4$) nanocomposite: Kinetics and isotherm study. *Environ. Sci. Pollut. Res.* **2020**, *27*, 37977–37988. [CrossRef] [PubMed]
79. Wang, Q.; O'Hare, D. Recent Advances in the Synthesis and Application of Layered Double Hydroxide (LDH) Nanosheets. *Chem. Rev.* **2012**, *112*, 4124–4155. [CrossRef] [PubMed]
80. Zaghouane-Boudiaf, H.; Boutahala, M.; Arab, L. Removal of methyl orange from aqueous solution by uncalcined and calcined MgNiAl layered double hydroxides (LDHs). *Chem. Eng. J.* **2012**, *187*, 142–149. [CrossRef]

81. Alagha, O.; Manzar, M.S.; Zubair, M.; Anil, I.; Mu'azu, N.D.; Qureshi, A. Magnetic Mg-Fe/LDH Intercalated Activated Carbon Composites for Nitrate and Phosphate Removal from Wastewater: Insight into Behavior and Mechanisms. *Nanomaterials* **2020**, *10*, 1361. [CrossRef]
82. Zhang, T.; Dong, L.; Du, J.; Qian, C.; Wang, Y. CuO and CeO_2 assisted Fe_2O_3/attapulgite catalyst for heterogeneous Fenton-like oxidation of methylene blue. *RSC Adv.* **2020**, *10*, 23431–23439. [CrossRef]
83. Xu, B.-D.; Li, D.-C.; Qian, T.-T.; Jiang, H. Boosting the activity and environmental stability of nanoscale zero-valent iron by montmorillonite supporting and sulfidation treatment. *Chem. Eng. J.* **2020**, *387*, 124063. [CrossRef]
84. Li, T.; Wang, X.; Chen, Y.; Liang, J.; Zhou, L. Producing, O.H.; SO_4- and O_2- in heterogeneous Fenton reaction induced by Fe_3O_4-modified schwertmannite. *Chem. Eng. J.* **2020**, *393*, 124735. [CrossRef]
85. Tan, Y.; Li, C.; Sun, Z.; Bian, R.; Dong, X.; Zhang, X.; Zheng, S. Natural diatomite mediated spherically monodispersed $CoFe_2O_4$ nanoparticles for efficient catalytic oxidation of bisphenol A through activating peroxymonosulfate. *Chem. Eng. J.* **2020**, *388*, 124386. [CrossRef]
86. Chen, Y.; Feng, L.; Sadeghzadeh, S.M. Reduction of 4-nitrophenol and 2-nitroaniline using immobilized CoMn2O4 NPs on lignin supported on FPS. *RSC Adv.* **2020**, *10*, 19553–19561. [CrossRef]
87. Boycheva, S.; Zgureva, D.; Miteva, S.; Marinov, I.; Behunová, D.M.; Trendafilova, I.; Popova, M.; Václaviková, M. Studies on the Potential of Nonmodified and Metal Oxide-Modified Coal Fly Ash Zeolites For Adsorption of Heavy Metals and Catalytic Degradation of Organics for Waste Water Recovery. *Processes* **2020**, *8*, 778. [CrossRef]
88. Jee, S.-C.; Kim, M.; Shinde, S.K.; Ghodake, G.S.; Sung, J.-S.; Kadam, A.A. Assembling ZnO and Fe_3O_4 nanostructures on halloysite nanotubes for anti-bacterial assessments. *Appl. Surf. Sci.* **2020**, *509*, 145358. [CrossRef]
89. Rashid, M.H.; Mandal, T.K. Synthesis and Catalytic Application of Nanostructured Silver Dendrites. *J. Phys. Chem. C* **2007**, *111*, 16750–16760. [CrossRef]
90. Dong, Z.; Le, X.; Li, X.; Zhang, W.; Dong, C.; Ma, J. Silver nanoparticles immobilized on fibrous nano-silica as highly efficient and recyclable heterogeneous catalyst for reduction of 4-nitrophenol and 2-nitroaniline. *Appl. Catal. B Environ.* **2014**, *158–159*, 129–135. [CrossRef]
91. Tang, S.; Vongehr, S.; Meng, X. Carbon Spheres with Controllable Silver Nanoparticle Doping. *J. Phys. Chem. C* **2010**, *114*, 977–982. [CrossRef]
92. Sahiner, N.; Ozay, H.; Ozay, O.; Aktas, N. A soft hydrogel reactor for cobalt nanoparticle preparation and use in the reduction of nitrophenols. *Appl. Catal. B Environ.* **2010**, *101*, 137–143. [CrossRef]
93. Luciano, A.J.R.; de Sousa Soletti, L.; Ferreira, M.E.C.; Cusioli, L.F.; de Andrade, M.B.; Bergamasco, R.; Yamaguchi, N.U. Manganese ferrite dispersed over graphene sand composite for methylene blue photocatalytic degradation. *J. Environ. Chem. Eng.* **2020**, *8*, 104191. [CrossRef]
94. Gonçalves, A.H.A.; Siciliano, P.H.C.; Alves, O.C.; Cesar, D.V.; Henriques, C.A.; Gaspar, A.B. Synthesis of a Magnetic Fe_3O_4/RGO Composite for the Rapid Photo-Fenton Discoloration of Indigo Carmine Dye. *Top. Catal.* **2020**. [CrossRef]
95. Ferreira, F.N.; Benevides, A.P.; Cesar, D.V.; Luna, A.S.; de Gois, J.S. Magnetic solid-phase extraction and pre-concentration of 17β-estradiol and 17α-ethinylestradiol in tap water using maghemite-graphene oxide nanoparticles and determination via HPLC with a fluorescence detector. *Microchem. J.* **2020**, *157*, 104947. [CrossRef]
96. Bao, S.; Yang, W.; Wang, Y.; Yu, Y.; Sun, Y. One-pot synthesis of magnetic graphene oxide composites as an efficient and recoverable adsorbent for Cd(II) and Pb(II) removal from aqueous solution. *J. Hazard. Mater.* **2020**, *381*, 120914. [CrossRef]
97. Liu, Q.; Hu, S.; Yang, Z.; Zhang, X.; Ge, J. Green Synthesis of Composite Graphene Aerogels with Robust Magnetism for Effective Water Remediation. *Materials* **2019**, *12*, 4106. [CrossRef] [PubMed]
98. Li, X.; Zhang, D.; Liu, Z.; Lyu, C.; Niu, S.; Dong, Z.; Lyu, C. Enhanced catalytic oxidation of benzotriazole via peroxymonosulfate activated by $CoFe_2O_4$ supported onto nitrogen-doped three-dimensional graphene aerogels. *Chem. Eng. J.* **2020**, *400*, 125897. [CrossRef]
99. Liu, Z.; Gao, Z.; Xu, L.; Hu, F. Polypyrrole modified magnetic reduced graphene oxide composites: Synthesis, characterization and application for selective lead adsorption. *RSC Adv.* **2020**, *10*, 17524–17533. [CrossRef]

100. Sun, Y.; Lei, J.; Wang, Y.; Tang, Q.; Kang, C. Fabrication of a magnetic ternary $ZnFe_2O_4/TiO_2$/RGO Z-scheme system with efficient photocatalytic activity and easy recyclability. *RSC Adv.* **2020**, *10*, 17293–17301. [CrossRef]
101. Rong, Y.; Huang, Y.; Jin, P.; Yang, C.; Zhong, Z.; Dong, C.; Liang, W. Highly efficient removal of cationic, anionic and neutral dyes by hierarchically porous structured three-dimensional magnetic sulfur/nitrogen co-doped reduced graphene oxide nanohybrid. *J. Water Process Eng.* **2020**, *37*, 101345. [CrossRef]
102. Zhang, J.; Kang, M.; Zhou, Y.; Ma, C.; Ning, F.; Qiu, Z. Facile synthesis of polyethyleneimine modified magnetic graphite: An effective adsorbent for the removal of humic acid from aqueous solution. *Mater. Chem. Phys.* **2020**, *255*, 123549. [CrossRef]
103. Zhang, X.; Cui, C.; Wang, Y.; Chang, J.; Ma, D.; Wang, J. An efficient method for removal of pentachlorophenol using adsorption and microwave regeneration with different magnetic carbon nanotubes. *Water Sci. Technol.* **2020**, *81*, 585–595. [CrossRef]
104. Wu, X.; Xu, G.; Wang, J. Ultrasound-assisted coagulation for Microcystis aeruginosa removal using Fe_3O_4-loaded carbon nanotubes. *RSC Adv.* **2020**, *10*, 13525–13531. [CrossRef]
105. Chen, Y.; Yang, Z.; Liu, Y.; Liu, Y. Fenton-like degradation of sulfamerazine at nearly neutral pH using Fe-Cu-CNTs and Al0-CNTs for in-situ generation of H_2O_2/OH/O_2−. *Chem. Eng. J.* **2020**, *396*, 125329. [CrossRef]
106. Manickam-Periyaraman, P.; Espinosa, J.C.; Ferrer, B.; Subramanian, S.; Álvaro, M.; García, H.; Navalón, S. Bimetallic iron-copper oxide nanoparticles supported on nanometric diamond as efficient and stable sunlight-assisted Fenton photocatalyst. *Chem. Eng. J.* **2020**, *393*, 124770. [CrossRef]
107. Zenobio, J.E.; Modiri-Gharehveran, M.; de Perre, C.; Vecitis, C.D.; Lee, L.S. Reductive transformation of perfluorooctanesulfonate by nNiFe0-Activated carbon. *J. Hazard. Mater.* **2020**, *397*, 122782. [CrossRef] [PubMed]
108. Xu, J.; Liu, X.; Cao, Z.; Bai, W.; Shi, Q.; Yang, Y. Fast degradation, large capacity, and high electron efficiency of chloramphenicol removal by different carbon-supported nanoscale zerovalent iron. *J. Hazard. Mater.* **2020**, *384*, 121253. [CrossRef] [PubMed]
109. EPA. Drinking Water Health Advisories for PFOA and PFOS. Gr. Water Drink. Water. 2020. Available online: https://www.epa.gov/ground-water-and-drinking-water/drinking-water-health-advisories-pfoa-and-pfos#:~{}:text=ToprovideAmericans%2Cincludingthe,at70partspertrillion (accessed on 9 September 2020).
110. WHO. Fluoride in Drinking-water. In Backgr. Doc. Dev. WHO Guidel. Drink. Qual. 2004. Available online: https://www.who.int/water_sanitation_health/dwq/chemicals/fluoride.pdf?ua=1 (accessed on 9 September 2020).
111. WHO. Sulfate in Drinking-water. In Backgr. Doc. Dev. WHO Guidel. Drink. Qual. 2004. Available online: https://www.who.int/water_sanitation_health/dwq/chemicals/sulfate.pdf (accessed on 9 September 2020).
112. Nkinahamira, F.; Alsbaiee, A.; Zeng, Q.; Li, Y.; Zhang, Y.; Feng, M.; Yu, C.-P.; Sun, Q. Selective and fast recovery of rare earth elements from industrial wastewater by porous β-cyclodextrin and magnetic β-cyclodextrin polymers. *Water Res.* **2020**, *181*, 115857. [CrossRef]
113. Chu, F.-J.; Wan, T.-J.; Chen, H.; Wu, C.-H.; Kao, P.-M. Magnetophoretic Harvesting of Nannochloropsis oculata Using Iron Oxide Immobilized Beads. *Water* **2020**, *12*, 236. [CrossRef]
114. Jacukowicz-Sobala, I.; Ociński, D.; Mazur, P.; Stanisławska, E.; Kociołek-Balawejder, E. Cu(II)-Fe(III) oxide doped anion exchangers–Multifunctional composites for arsenite removal from water via As(III) adsorption and oxidation. *J. Hazard. Mater.* **2020**, *394*, 122527. [CrossRef]
115. Elwakeel, K.Z.; Shahat, A.; Al-Bogami, A.S.; Wijesiri, B.; Goonetilleke, A. The synergistic effect of ultrasound power and magnetite incorporation on the sorption/desorption behavior of Cr(VI) and As(V) oxoanions in an aqueous system. *J. Colloid Interface Sci.* **2020**, *569*, 76–88. [CrossRef]
116. Wang, J.; Zhang, Q.; Liu, J.; Ji, X.; Ma, J.; Tian, G. Preparation and excellent adsorption of water pollution dyes over magnetic Fe3O4/C nanoparticles with hollow grape cluster morphology. *J. Nanopart. Res.* **2020**, *22*, 196. [CrossRef]
117. Aliahmadipoor, P.; Ghazanfari, D.; Gohari, R.J.; Akhgar, M.R. Preparation of PVDF/FMBO composite electrospun nanofiber for effective arsenate removal from water. *RSC Adv.* **2020**, *10*, 24653–24662. [CrossRef]

118. Ahmad, M.; Wu, F.; Cui, Y.; Zhang, Q.; Zhang, B. Preparation of Novel Bifunctional Magnetic Tubular Nanofibers and Their Application in Efficient and Irreversible Uranium Trap from Aqueous Solution. *ACS Sustain. Chem. Eng.* **2020**, *8*, 7825–7838. [CrossRef]
119. Sun, F.; He, J.; Wu, P.; Zeng, Q.; Liu, C.; Jiang, W. Magnetic photocatalyst $CoFe_2O_4$-Ag_2O with magnetic aggregation bed photocatalytic reactor for continuous photodegradation of methyl orange. *Chem. Eng. J.* **2020**, *397*, 125397. [CrossRef]
120. Abou Hammad, A.B.; El Nahwary, A.M.; Hemdan, B.A.; Abia, A.L.K. Nanoceramics and novel functionalized silicate-based magnetic nanocomposites as substitutional disinfectants for water and wastewater purification. *Environ. Sci. Pollut. Res.* **2020**, *27*, 26668–26680. [CrossRef] [PubMed]
121. Meena, S.; Anantharaju, K.S.; Vidya, Y.S.; Renuka, L.; Malini, S.; Sharma, S.C.; Nagabhushana, H. $MnFe_2O_4/ZrO_2$ nanocomposite as an efficient magnetically separable photocatalyst with good response to sunlight: Preparation, characterization and catalytic mechanism. *SN Appl. Sci.* **2020**, *2*, 328. [CrossRef]
122. Nicola, R.; Costişor, O.; Ciopec, M.; Negrea, A.; Lazău, R.; Ianăşi, C.; Picioruş, E.-M.; Len, A.; Almásy, L.; Szerb, E.I.; et al. Silica-Coated Magnetic Nanocomposites for Pb^{2+} Removal from Aqueous Solution. *Appl. Sci.* **2020**, *10*, 2726. [CrossRef]
123. Lv, Y.; Huang, S.; Huang, G.; Liu, Y.; Yang, G.; Lin, C.; Xiao, G.; Wang, Y.; Liu, M. Remediation of organic arsenic contaminants with heterogeneous Fenton process mediated by SiO_2-coated nano zero-valent iron. *Environ. Sci. Pollut. Res.* **2020**, *27*, 12017–12029. [CrossRef]
124. Wan, H.; Islam, M.S.; Qian, D.; Ormsbee, L.; Bhattacharyya, D. Reductive degradation of CCl4 by sulfidized Fe and Pd-Fe nanoparticles: Kinetics, longevity, and morphology aspects. *Chem. Eng. J.* **2020**, *394*, 125013. [CrossRef]
125. Rahdar, A.; Rahdar, S.; Labuto, G. Environmentally friendly synthesis of Fe_2O_3@SiO_2 nanocomposite: Characterization and application as an adsorbent to aniline removal from aqueous solution. *Environ. Sci. Pollut. Res.* **2020**, *27*, 9181–9191. [CrossRef]
126. Khodadadi, M.; Al-Musawi, T.J.; Kamani, H.; Silva, M.F.; Panahi, A.H. The practical utility of the synthesis $FeNi_3$@SiO_2@TiO_2 magnetic nanoparticles as an efficient photocatalyst for the humic acid degradation. *Chemosphere* **2020**, *239*, 124723. [CrossRef]
127. Nasseh, N.; Hossein Panahi, A.; Esmati, M.; Daglioglu, N.; Asadi, A.; Rajati, H.; Khodadoost, F. Enhanced photocatalytic degradation of tetracycline from aqueous solution by a novel magnetically separable $FeNi_3/SiO_2$/ZnO nano-composite under simulated sunlight: Efficiency, stability, and kinetic studies. *J. Mol. Liq.* **2020**, *301*, 112434. [CrossRef]
128. Khodadadi, M.; Hossein Panahi, A.; Al-Musawi, T.J.; Ehrampoush, M.H.; Mahvi, A.H. The catalytic activity of $FeNi_3$@SiO_2 magnetic nanoparticles for the degradation of tetracycline in the heterogeneous Fenton-like treatment method. *J. Water Process Eng.* **2019**, *32*, 100943. [CrossRef]
129. Nasseh, N.; Taghavi, L.; Barikbin, B.; Nasseri, M.A.; Allahresani, A. $FeNi_3/SiO_2$ magnetic nanocomposite as an efficient and recyclable heterogeneous fenton-like catalyst for the oxidation of metronidazole in neutral environments: Adsorption and degradation studies. *Compos. Part B Eng.* **2019**, *166*, 328–340. [CrossRef]
130. Tao, Q.; Huang, X.; Bi, J.; Wei, R.; Xie, C.; Zhou, Y.; Yu, L.; Hao, H.; Wang, J. Aerobic Oil-Phase Cyclic Magnetic Adsorption to Synthesize 1D Fe_2O_3@TiO_2 Nanotube Composites for Enhanced Visible-Light Photocatalytic Degradation. *Nanomaterials* **2020**, *10*, 1345.
131. Boruah, P.K.; Yadav, A.; Das, M.R. Magnetic mixed metal oxide nanomaterials derived from industrial waste and its photocatalytic applications in environmental remediation. *J. Environ. Chem. Eng.* **2020**, *8*, 104297. [CrossRef]
132. Mohan, H.; Lim, J.-M.; Lee, S.-W.; Jang, J.S.; Park, Y.-J.; Seralathan, K.-K.; Oh, B.-T. Enhanced visible light photocatalysis with E-waste-based V2O5/zinc–ferrite: BTEX degradation and mechanism. *J. Chem. Technol. Biotechnol.* **2020**. [CrossRef]
133. Nikić, J.; Watson, M.A.; Isakovski, M.K.; Tubić, A.; Šolić, M.; Kordić, B.; Agbaba, J. Synthesis, characterization and application of magnetic nanoparticles modified with Fe-Mn binary oxide for enhanced removal of As(III) and As(V). *Environ. Technol.* **2019**, 1–13. [CrossRef]
134. Krishna, S.; Sathishkumar, P.; Pugazhenthiran, N.; Guesh, K.; Mangalaraja, R.V.; Kumaran, S.; Gracia-Pinilla, M.A.; Anandan, S. Magnetically recyclable $CoFe_2O_4$/ZnO nanocatalysts for the efficient catalytic degradation of Acid Blue 113 under ambient conditions. *RSC Adv.* **2020**, *10*, 16473–16480. [CrossRef]

135. Massoud-Sharifi, A.; Kara, G.K.; Rabbani, M. $CuFe_2O_4$@CuO: A Magnetic Composite Synthesized by Ultrasound Irradiation and Degradation of Methylene Blue on Its Surface in the Presence of Sunlight. *Proceedings* **2020**, *48*, 17.
136. Tian, C.; Li, J.; Li, Q.; Nie, Y.; Tian, X.; Dai, C.; Yang, C.; Zhou, Z.; Wang, Y. Surface weak acid-base pair of $FeOOH/Al_2O_3$ for enhanced peroxymonosulfate activation in degradation of humic substances from water. *Chem. Eng. J.* **2020**, *387*, 124064. [CrossRef]
137. Ashtiani, S.; Khoshnamvand, M.; Shaliutina-Kolešová, A.; Bouša, D.; Sofer, Z.; Friess, K. $Co_{0.5}Ni_{0.5}FeCrO_4$ spinel nanoparticles decorated with UiO-66-based metal-organic frameworks grafted onto GO and O-SWCNT for gas adsorption and water purification. *Chemosphere* **2020**, *255*, 126966. [CrossRef]
138. Fang, Y.; Wen, J.; Zhang, H.; Wang, Q.; Hu, X. Enhancing Cr(VI) reduction and immobilization by magnetic core-shell structured NZVI@MOF derivative hybrids. *Environ. Pollut.* **2020**, *260*, 114021. [CrossRef]
139. Khedkar, C.V.; Khupse, N.D.; Thombare, B.R.; Dusane, P.R.; Lole, G.; Devan, R.S.; Deshpande, A.S.; Patil, S.I. Magnetically separable Ag-Fe3O4 catalyst for the reduction of organic dyes. *Chem. Phys. Lett.* **2020**, *742*, 137131. [CrossRef]
140. Gallo-Cordova, A.; Lemus, J.; Palomares, F.J.; Morales, M.P.; Mazarío, E. Superparamagnetic nanosorbent for water purification: Assessment of the adsorptive removal of lead and methyl orange from aqueous solutions. *Sci. Total Environ.* **2020**, *711*, 134644. [CrossRef] [PubMed]
141. Xing, Y.; Bai, X.-H.; Gong, Y.; Peng, M.-L.; Zhang, Y.-Y.; Ma, X.-R.; Zhang, Y. Enhanced catalytic properties of Fe_3O_4/Ag magnetic microspheres synthesized by a novel thermal co-reduction method. *J. Magn. Magn. Mater.* **2020**, *510*, 166951. [CrossRef]
142. Zhang, A.; Li, X.; Xing, J.; Xu, G. Adsorption of potentially toxic elements in water by modified biochar: A review. *J. Environ. Chem. Eng.* **2020**, *8*, 104196. [CrossRef]
143. Abegunde, S.M.; Idowu, K.S.; Sulaimon, A.O. Plant-Mediated Iron Nanoparticles and their Applications as Adsorbents for Water Treatment–A Review. *J. Chem. Rev.* **2020**, *2*, 103–113. [CrossRef]
144. Gautam, R.K.; Tiwari, I. Humic acid functionalized magnetic nanomaterials for remediation of dye wastewater under ultrasonication: Application in real water samples, recycling and reuse of nanosorbents. *Chemosphere* **2020**, *245*, 125553. [CrossRef] [PubMed]
145. Gonçalves, N.P.F.; Minella, M.; Fabbri, D.; Calza, P.; Malitesta, C.; Mazzotta, E.; Bianco Prevot, A. Humic acid coated magnetic particles as highly efficient heterogeneous photo-Fenton materials for wastewater treatments. *Chem. Eng. J.* **2020**, *390*, 124619. [CrossRef]
146. Hu, L.; Guang, C.; Liu, Y.; Su, Z.; Gong, S.; Yao, Y.; Wang, Y. Adsorption behavior of dyes from an aqueous solution onto composite magnetic lignin adsorbent. *Chemosphere* **2020**, *246*, 125757. [CrossRef]
147. Chen, H.; Xu, F.; Chen, Z.; Jiang, O.; Gustave, W.; Tang, X. Arsenic and cadmium removal from water by a calcium-modified and starch-stabilized ferromanganese binary oxide. *J. Environ. Sci.* **2020**, *96*, 186–193. [CrossRef]
148. Patil, S.A.; Kumbhar, P.D.; Patil, S.K.; Vadiyar, M.M.; Suryawanshi, U.P.; Jambhale, C.L.; Anuse, M.A.; Kim, J.H.; Kolekar, S.S. Dynamic adsorption of toxic indigo carmine dye on bio-inspired synthesised Fe3O4 nanoparticles: Kinetic and thermodynamic study. *Int. J. Environ. Anal. Chem.* **2020**, 1–23. [CrossRef]
149. Egorin, A.; Tokar, E.; Matskevich, A.; Ivanov, N.; Tkachenko, I.; Sokolnitskaya, T.; Zemskova, L. Composite Magnetic Sorbents Based on Iron Oxides in Different Polymer Matrices: Comparison and Application for Removal of Strontium. *Biomimetics* **2020**, *5*, 22. [CrossRef] [PubMed]
150. He, Y.; Wu, P.; Li, G.; Li, L.; Yi, J.; Wang, S.; Lu, S.; Ding, P.; Chen, C.; Pan, H. Optimization on preparation of Fe_3O_4/chitosan as potential matrix material for the removal of microcystin-LR and its evaluation of adsorption properties. *Int. J. Biol. Macromol.* **2020**, *156*, 1574–1583. [CrossRef] [PubMed]
151. Lobo, C.; Castellari, J.; Colman Lerner, J.; Bertola, N.; Zaritzky, N. Functional iron chitosan microspheres synthesized by ionotropic gelation for the removal of arsenic (V) from water. *Int. J. Biol. Macromol.* **2020**, *164*, 1575–1583. [CrossRef] [PubMed]
152. Lei, C.; Wang, C.; Chen, W.; He, M.; Huang, B. Polyaniline@magnetic chitosan nanomaterials for highly efficient simultaneous adsorption and in-situ chemical reduction of hexavalent chromium: Removal efficacy and mechanisms. *Sci. Total Environ.* **2020**, *733*, 139316. [CrossRef]
153. Zhang, M.; Zhang, Z.; Peng, Y.; Feng, L.; Li, X.; Zhao, C.; Sarfaraz, K. Novel cationic polymer modified magnetic chitosan beads for efficient adsorption of heavy metals and dyes over a wide pH range. *Int. J. Biol. Macromol.* **2020**, *156*, 289–301. [CrossRef]

154. Yu, S.; Wang, J.; Cui, J. Preparation of a novel chitosan-based magnetic adsorbent CTS@SnO_2@Fe_3O_4 for effective treatment of dye wastewater. *Int. J. Biol. Macromol.* **2020**, *156*, 1474–1482. [CrossRef]
155. Silva, M.A.; Rocha, C.V.; Gallo, J.; Felgueiras, H.P.; Pessoa de Amorim, M.T. Porous composites based on cellulose acetate and alfa-hematite with optical and antimicrobial properties. *Carbohydr. Polym.* **2020**, *241*, 116362. [CrossRef]
156. Peng, B.; Zhou, R.; Chen, Y.; Tu, S.; Yin, Y.; Ye, L. Immobilization of nano-zero-valent irons by carboxylated cellulose nanocrystals for wastewater remediation. *Front. Chem. Sci. Eng.* **2020**. [CrossRef]
157. Muniz, E.P.; de Assunção, L.S.D.; de Souza, L.M.; Ribeiro, J.J.K.; Marques, W.P.; Pereira, R.D.; Porto, P.S.S.; Proveti, J.R.C.; Passamani, E.C. On cobalt ferrite production by sol-gel from orange fruit residue by three related procedures and its application in oil removal. *J. Clean. Prod.* **2020**, *265*, 121712. [CrossRef]
158. Liu, Q.; Ma, P.; Liu, P.; Li, H.; Han, X.; Liu, L.; Zou, W. Green synthesis of stable Fe,Cu oxide nanocomposites from loquat leaf extracts for removal of Norfloxacin and Ciprofloxacin. *Water Sci. Technol.* **2020**, *81*, 694–708. [CrossRef]
159. Din, M.I.; Jabbar, S.; Najeeb, J.; Khalid, R.; Ghaffar, T.; Arshad, M.; Khan, S.A.; Ali, S. Green synthesis of zinc ferrite nanoparticles for photocatalysis of methylene blue. *Int. J. Phytoremediat.* **2020**, 1–8. [CrossRef] [PubMed]
160. Dwivedi, L.M.; Shukla, N.; Baranwal, K.; Gupta, S.; Siddique, S.; Singh, V. Gum Acacia Modified Ni Doped CuO Nanoparticles: An Excellent Antibacterial Material. *J. Clust. Sci.* **2020**. [CrossRef]
161. Atta, A.M.; Mohamed, N.H.; Hegazy, A.K.; Moustafa, Y.M.; Mohamed, R.R.; Safwat, G.; Diab, A.A. Green Technology for Remediation of Water Polluted with Petroleum Crude Oil: Using of Eichhornia crassipes (Mart.) Solms Combined with Magnetic Nanoparticles Capped with Myrrh Resources of Saudi Arabia. *Nanomaterials* **2020**, *10*, 262. [CrossRef] [PubMed]
162. Nikić, J.; Tubić, A.; Watson, M.; Maletić, S.; Šolić, M.; Majkić, T.; Agbaba, J. Arsenic Removal from Water by Green Synthesized Magnetic Nanoparticles. *Water* **2019**, *11*, 2520. [CrossRef]
163. Afridi, M.N.; Lee, W.-H.; Kim, J.-O. Application of synthesized bovine serum albumin-magnetic iron oxide for phosphate recovery. *J. Ind. Eng. Chem.* **2020**, *86*, 113–122. [CrossRef]
164. Zhou, L.; Li, A.; Ma, F.; Zhao, H.; Deng, F.; Pi, S.; Tang, A.; Yang, J. Combining high electron transfer efficiency and oxidation resistance in nZVI with coatings of microbial extracellular polymeric substances to enhance Sb(V) reduction and adsorption. *Chem. Eng. J.* **2020**, *395*, 125168. [CrossRef]
165. Zhang, D.; Li, Y.; Sun, A.; Tong, S.; Jiang, X.; Mu, Y.; Li, J.; Han, W.; Sun, X.; Wang, L.; et al. Optimization ofS/Fe ratio for enhanced nitrobenzene biological removal in anaerobicSystem amended withSulfide-modified nanoscale zerovalent iron. *Chemosphere* **2020**, *247*, 125832. [CrossRef] [PubMed]
166. Wu, Q.; Ye, X.; Lv, Y.; Pei, R.; Wu, M.; Liu, M. Lignin-based magnetic activated carbon for p-arsanilic acid removal: Applications and absorption mechanisms. *Chemosphere* **2020**, *258*, 127276. [CrossRef]
167. Oladebeye, A.O. Potentials of Starch Nanoparticles Jack Bean (Canavalia ensiformis) Coprecipitated with Iron (II, III) Oxide. *Int. Res. J. Pure Appl. Chem.* **2020**, *21*, 17–24. [CrossRef]
168. Yildiz, A.; Vatansever Bayramol, D.; Atav, R.; Ağirgan, A.Ö.; Aydin Kurç, M.; Ergünay, U.; Mayer, C.; Hadimani, R.L. Synthesis and characterization of Fe3O4@Cs@Ag nanocomposite and its use in the production of magnetic and antibacterial nanofibrous membranes. *Appl. Surf. Sci.* **2020**, *521*, 146332. [CrossRef]
169. Mu, C.; Zhang, L.; Zhang, X.; Zhong, L.; Li, Y. Selective adsorption of Ag (I) from aqueous solutions using Chitosan/polydopamine@C@magnetic fly ash adsorbent beads. *J. Hazard. Mater.* **2020**, *381*, 120943. [CrossRef] [PubMed]
170. Liu, K.; Li, F.; Cui, J.; Yang, S.; Fang, L. Simultaneous removal of Cd(II) and As(III) by graphene-like biochar-supported zero-valent iron from irrigation waters under aerobic conditions: Synergistic effects and mechanisms. *J. Hazard. Mater.* **2020**, *395*, 122623. [CrossRef] [PubMed]
171. Zhang, Y.; Jiao, X.; Liu, N.; Lv, J.; Yang, Y. Enhanced removal of aqueous Cr(VI) by a green synthesized nanoscale zero-valent iron supported on oak wood biochar. *Chemosphere* **2020**, *245*, 125542. [CrossRef] [PubMed]
172. Qian, L.; Zhang, W.; Yan, J.; Han, L.; Chen, Y.; Ouyang, D.; Chen, M. Nanoscale zero-valent iron supported by biochars produced at different temperatures: Synthesis mechanism and effect on Cr(VI) removal. *Environ. Pollut.* **2017**, *223*, 153–160. [CrossRef] [PubMed]

173. Shang, X.; Yang, L.; Ouyang, D.; Zhang, B.; Zhang, W.; Gu, M.; Li, J.; Chen, M.; Huang, L.; Qian, L. Enhanced removal of 1,2,4-trichlorobenzene by modified biochar supported nanoscale zero-valent iron and palladium. *Chemosphere* **2020**, *249*, 126518. [CrossRef]
174. Yan, J.; Yang, L.; Qian, L.; Han, L.; Chen, M. Nano-magnetite supported by biochar pyrolyzed at different temperatures as hydrogen peroxide activator: Synthesis mechanism and the effects on ethylbenzene removal. *Environ. Pollut.* **2020**, *261*, 114020. [CrossRef]
175. Wei, D.; Li, B.; Luo, L.; Zheng, Y.; Huang, L.; Zhang, J.; Yang, Y.; Huang, H. Simultaneous adsorption and oxidation of antimonite onto nano zero-valent iron sludge-based biochar: Indispensable role of reactive oxygen species and redox-active moieties. *J. Hazard. Mater.* **2020**, *391*, 122057. [CrossRef]
176. Yang, Z.; Li, Y.; Zhang, X.; Cui, X.; He, S.; Liang, H.; Ding, A. Sludge activated carbon-based $CoFe_2O_4$-SAC nanocomposites used as heterogeneous catalysts for degrading antibiotic norfloxacin through activating peroxymonosulfate. *Chem. Eng. J.* **2020**, *384*, 123319. [CrossRef]
177. Zhang, S.; Lyu, H.; Tang, J.; Song, B.; Zhen, M.; Liu, X. A novel biochar supported CMC stabilized nano zero-valent iron composite for hexavalent chromium removal from water. *Chemosphere* **2019**, *217*, 686–694. [CrossRef]
178. Li, Y.; Ma, S.; Xu, S.; Fu, H.; Li, Z.; Li, K.; Sheng, K.; Du, J.; Lu, X.; Li, X.; et al. Novel magnetic biochar as an activator for peroxymonosulfate to degrade bisphenol A: Emphasizing the synergistic effect between graphitized structure and $CoFe_2O_4$. *Chem. Eng. J.* **2020**, *387*, 124094. [CrossRef]
179. Liu, C.; Chen, L.; Ding, D.; Cai, T. From rice straw to magnetically recoverable nitrogen doped biochar: Efficient activation of peroxymonosulfate for the degradation of metolachlor. *Appl. Catal. B Environ.* **2019**, *254*, 312–320. [CrossRef]
180. Han, L.; Yan, J.; Qian, L.; Zhang, W.; Chen, M. Multifunctional Pd/Fe-biochar composites for the complete removal of trichlorobenzene and its degradation products. *J. Environ. Manag.* **2019**, *245*, 238–244. [CrossRef]
181. Qian, L.; Liu, S.; Zhang, W.; Chen, Y.; Ouyang, D.; Han, L.; Yan, J.; Chen, M. Enhanced reduction and adsorption of hexavalent chromium by palladium and silicon rich biochar supported nanoscale zero-valent iron. *J. Colloid Interface Sci.* **2019**, *533*, 428–436. [CrossRef]
182. Zhu, S.; Xu, Y.; Zhu, Z.; Liu, Z.; Wang, W. Activation of peroxymonosulfate by magnetic Co-Fe/SiO_2 layered catalyst derived from iron sludge for ciprofloxacin degradation. *Chem. Eng. J.* **2020**, *384*, 123298. [CrossRef]
183. Chen, R.-H.; Cheng, Y.-Y.; Wang, P.; Liu, Z.-M.; Wang, Y.-G.; Wang, Y.-Y. High efficient removal and mineralization of Cr(VI) from water by functionalized magnetic fungus nanocomposites. *J. Cent. South Univ.* **2020**, *27*, 1503–1514. [CrossRef]
184. Debs, K.B.; Cardona, D.S.; da Silva, H.D.T.; Nassar, N.N.; Carrilho, E.N.V.M.; Haddad, P.S.; Labuto, G. Oil spill cleanup employing magnetite nanoparticles and yeast-based magnetic bionanocomposite. *J. Environ. Manag.* **2019**, *230*, 405–412. [CrossRef]
185. Cardona, D.S.; Debs, K.B.; Lemos, S.G.; Vitale, G.; Nassar, N.N.; Carrilho, E.N.V.M.; Semensatto, D.; Labuto, G. A comparison study of cleanup techniques for oil spill treatment using magnetic nanomaterials. *J. Environ. Manag.* **2019**, *242*, 362–371. [CrossRef]
186. Ozdemir, S.; Kılınc, E.; Yalcin, M.S.; Soylak, M.; Sen, F. A new magnetized thermophilic bacteria to preconcentrate uranium and thorium from environmental samples through magnetic solid-phase extraction. *J. Pharm. Biomed. Anal.* **2020**, *186*, 113315. [CrossRef]
187. Lu, J.; Zhang, C.; Wu, J. One-pot synthesis of magnetic algal carbon/sulfidated nanoscale zerovalent iron composites for removal of bromated disinfection by-product. *Chemosphere* **2020**, *250*, 126257. [CrossRef]
188. Li, H.; Chen, S.; Ren, L.Y.; Zhou, L.Y.; Tan, X.J.; Zhu, Y.; Belver, C.; Bedia, J.; Yang, J. Biochar mediates activation of aged nanoscale ZVI by Shewanella putrefaciens CN32 to enhance the degradation of Pentachlorophenol. *Chem. Eng. J.* **2019**, *368*, 148–156. [CrossRef]
189. Shi, Z.; Shen, W.; Yang, K.; Zheng, N.; Jiang, X.; Liu, L.; Yang, D.; Zhang, L.; Ai, Z.; Xie, B. Hexavalent chromium removal by a new composite system of dissimilatory iron reduction bacteria Aeromonas hydrophila and nanoscale zero-valent iron. *Chem. Eng. J.* **2019**, *362*, 63–70. [CrossRef]
190. Özdemir, S.; Serkan Yalçın, M.; Kılınç, E. Preconcentrations of Ni(II) and Pb(II) from water and food samples by solid-phase extraction using Pleurotus ostreatus immobilized iron oxide nanoparticles. *Food Chem.* **2020**, *336*, 127675. [CrossRef] [PubMed]

191. Xie, Y.; Liu, H.; Li, H.; Tang, H.; Peng, H.; Xu, H. High-effectively degrade the di-(2-ethylhexyl) phthalate via biochemical system: Resistant bacterial flora and persulfate oxidation activated by BC@Fe_3O_4. *Environ. Pollut.* **2020**, *262*, 114100. [CrossRef] [PubMed]
192. Xia, Q.; Huo, M.; Hao, P.; Zheng, J.; An, Y. Transport of nano zerovalent iron (nZVI) coupling with Alcaligenes sp. strain in porous media. *RSC Adv.* **2020**, *10*, 24265–24272. [CrossRef]